Control and quality analysis of grid connected inverters output current

Victor Habermann Avila

Supervised by

Prof. Dr. Américo Vicente Teixeira Leite

Prof. Dr. Roger Gules

This work does not include notes and suggestions of the Juri

Bragança

2019-2020

Control and quality analysis of grid connected inverters output current

Victor Habermann Avila

Thesis presented in the School of Technology and Management
of the Polytechnic Institute of Bragança
to fulfill the requirements of a Master of Science Degree in
Renewable Energies and Energy Efficiency.

Supervised by
Prof. Dr. Américo Vicente Teixeira Leite
Prof. Dr. Roger Gules

This work does not include notes and suggestions of the Juri

Bragança
2019-2020

Acknowledgments

For my parents, who have always supported and guided me throughout my life. Without your advice, I would not be the person I am today. I couldn't have this experience in Portugal if it weren't by you.

To my beloved friends Alice Fey, Liege Aguiar, Rodolpho Fagundes and Sarah Gruetzmacher. I have grown a lot with our conversations on different subjects and I will keep forever in my mind the countless moments of joy that we had together. Without you, this time away from home would not have been so simple. I hope to meet you in Brazil soon.

To Professor Roger Gules, my advisor from UTFPR, who introduced me to power electronics. Your guidance was crucial to creating my interest in research. The opportunity to do this double degree was only possible with the experience I obtained working with you.

To Professor Vicente Leite, for being my advisor and helped me throughout this project. It has always been interesting to talk to you and hear your views on teaching and higher education. To my lab colleagues who, even though we were away due to the pandemic, we shared different knowledge and stories between work sessions. I would also like to acknowledge the LSE technicians for all the support and assistance provided during the work.

Finally, I would like to acknowledge Federal University of Technology - Paraná (UTFPR) and Polytechnic Institute of Bragança (IPB) for all the knowledge provided and for the opportunity to carry out this exchange.

Resumo

Com a expansão do uso de energias renováveis para a geração de energia elétrica, a matriz energética mundial tende a se tornar mais sustentável. O inversor é uma peça essencial em um sistema de geração elétrica a partir de fontes renováveis pois ele realiza a interface entre o sistema e a rede elétrica, fornecendo potência para a rede ou alimentando as cargas locais.

Com isso, o número de inversores conectados à rede tem se tornado cada vez maior, podendo injetar correntes com componentes harmônicas no sistema. Para que isso não afete a operação normal do sistema de distribuição, algumas regulamentações foram criadas definindo parâmetros de qualidade da energia a serem respeitados.

Sendo assim, o objetivo dessa dissertação é estudar e validar experimentalmente algumas técnicas de controle da corrente de saída de um inversor e topologias de filtro de saída, analisando o impacto desses componentes na qualidade da corrente injetada.

O modelo do conversor, bem como as estratégias de controle e os filtros de saída foram validados através de uma simulação em Simulink/MATLAB. Os testes experimentais realizaram-se em uma estrutura de potência de um conversor DC-AC implementada previamente no Laboratório de Sistemas Eletromecatrônicos (LSE). Para o controle da plataforma foi utilizado o sistema dSPACE, que permite uma programação simples da estrutura de controle, assim como a aquisição e processamento dos dados dos testes.

O objetivo desta dissertação foi atingido, obtendo resultados que apresentam a qualidade da corrente injetada sobre diferentes condições de teste e configurações do sistema. O controle proporcional ressonante com compensação harmônica apresentou melhores resultados na potência nominal, mas as demais estratégias aplicadas também se mostraram válidas para algumas aplicações.

Palavras-chave: inversor conectado à rede, harmônicos, qualidade da corrente, controle de corrente

Abstract

With the expansion of the use of renewable energies to generate electricity, the global energy matrix tends to become more sustainable. The inverter is an essential part of an electricity generation system from renewable sources, it interfaces between the system and the electrical network, supplying power to the grid or feeding the household loads.

As a result, the number of inverters connected to the grid has become increasingly larger, with the possibility of injecting current with harmonic components in the system. So that this does not affect the normal operation of the distribution system, some regulations were created defining energy quality parameters to be respected.

Therefore, the objective of this dissertation is to study and experimentally validate some techniques for controlling the output current of an inverter and output filter topologies, analyzing the impact of these components on the quality of the injected current.

The converter model, as well as the control strategies and the output filters were validated through a simulation in Simulink / MATLAB. For the experimental tests, a power structure of a DC-AC converter previously used in the LSE was used, which consists of a simple topology of a DC-DC converter and a complete bridge inverter. For the control of the platform the dSPACE system was used, which allows a simple programming of the control structure, as well as the acquisition and processing of the test data.

The objective of this dissertation was achieved, obtaining results that present the quality of the injected current under different test conditions and system configurations. The resonant proportional control with harmonic compensation showed better results in the nominal power, but the other applied strategies also proved to be valid for some applications.

Keywords: grid connected inverter, harmonics, current quality, current control

Contents

List of Tables

List of Figures

Acronyms

AC	Alternate current
DC	Direct current
DG	Distributed generation
EV	Electrical vehicle
HC	Harmonic compensator
IPB	Instituto Politécnico de Bragança
LSE	Electro Mechatronics System Laboratory
MG	Microgrids
MPPT	Maximum power point tracking
PID	Proportional-integral-derivative
PLL	Phase locked loop
PR	Proportional resonant
PV	Photovoltaic
PWM	Pulse width modulation
RE	Renewable energies
RTI	Real-time interface
THD	Total harmonic distortion
TRD	Total rated current distortion
VSI	Voltage source inverter
WT	Wind turbine

Chapter 1

Introduction

The share of renewable energy sources in the global energy matrix is increasing. The total amount is still very small, but it is already significant [1]. With that, wind turbines (WT) and photovoltaic (PV) systems are being applied in home installations along with microgrids (MG), generating clean energy and reducing the consumption from the grid. The concept of several low power generators distributed along the whole system is called a distributed generation (DG).

In some countries, like Portugal, the regulations of distributed energy do not stimulate the injection of power to the grid, but the self-consumption. Storage systems are a solution to these regulations problems. When the system is generating more than consuming, the exceeding power is stored in batteries. Thus, as an advantage, the system uses the stored power when the energy from the grid has a higher price [2].

Since MG systems usually have an energy storage element, it can operate even when the grid fails, disconnecting itself from the main grid and to supply home loads, operating in islanded mode. In this case, power quality parameters change as well as the whole system dynamic, requiring new control algorithms and safety parameters [3]. The inverter is an essential part of MGs, since it is the link between the source of energy and utility grid (or load). The control unit of it is responsible to comply with the requirements of the regulations mentioned above. Considering that, the focus of this work is the control algorithms and current quality of the inverter.

Along with the growth of renewable energy systems in houses, electrical vehicles (EVs) are increasing its share in the market. Most EVs nowadays only can charge themselves from the grid, but it is a trend that new models can also operate providing power to the grid. In these situations the power stored in the EVs' batteries can be injected to the grid, acting likewise as PV systems or battery inverters [4].

1.1 DG penetration and impacts on power quality

One drawback of renewable energy is the necessity to deal with the variations in power generation. Since the sources are dependent on the environmental conditions, the generated power is unstable and oscillates during short periods (minutes or hours), resulting in fluctuations of grid frequency and voltage [5].

Since PV systems generate direct current (DC) power, a transformation stage is necessary to convert this DC power to alternate current (AC) and inject on the grid. This is made through power electronic converters. Even on WT, which generates AC power, it is common to use power converters to control the generation and achieve maximum power. However, these converters may inject harmonics to the grid and, the power fluctuations from RE may result in voltage oscillations [6].

Most commercial single-phase inverters provide only active power to the grid. These inverters only inject current in phase to the voltage, which is imposed by the grid. However, inverter topologies can work as active power filters without any hardware adjustment, only updating control firmware to that function [7].

Furthermore, MGs with backup capacity have a good impact on grid voltage quality when the appropriate control is applied [8]. The perk of operating in islanded mode, besides providing service continuity to the customer, can relieve system stress during faults [9].

1.2 Power quality standards for inverters

There are several regulations, from international organizations and governments, that define some demands on power quality injected on the utility grid and how the system reacts to grid disturbances. To fulfill these requirements it is important to develop a good synchronization algorithm and current controller [10].

Since the beginning of distributed generation growth, several standards for interconnection and power quality of inverters were applied. IEEE 929-2000 is one of the oldest and

most applied standards over PV systems. After it, Underwriters Laboratory developed UL 1741, differentiating from other ULs that are focused on electric safety, 1741 focuses on grid performance of inverters [11].

For RE equipment in general, IEEE 1547-2003 applies an interconnection standard for all types of renewable energy technologies. It is based on works from other IEEE and IEC standards about grid interconnection and addresses systems up to 10 MW. This standard defines testing procedures, performance parameters, applications, and communication standards for DG systems [12].

Regarding current quality, IEEE 1547 presents two tables with the harmonic limits for each harmonic (h) and the total rated current distortion (TRD), summarized in Tables 1.1 and 1.2. The DC injection is limited to 0.5% of rated output current. It is also stated that the harmonics should be measured as recommended in IEEE 519 [13].

h	$h < 11$	$11 \leq h < 17$	$17 \leq h < 23$	$23 \leq h < 35$	$35 \leq h < 50$	**TRD**
%	4.0	2.0	1.5	0.6	0.3	5.0

Table 1.1: Odd harmonics limits.

h	$h = 2$	$h = 4$	$h = 6$
%	1.0	2.0	3.0

Table 1.2: Even harmonics limits.

1.3 Objectives

This work intends to study and analyze, with experimental validation, the impact of control algorithms and output filters in a grid-connected inverter output current. Using an existing power structure, test different control algorithms, and see its influence on current quality, as well as different combinations of low pass filters on inverter output. To achieve this objective, the secondary goals were:

- Study the state of art of current controllers for inverters;
- Study the most common output filters for inverters;
- Design and calculate component values for the filter;
- Simulate on Simulink/MATLAB the control of the inverter and the filter configurations;
- Test on experimental platform the studied controllers;
- Test filter variations on experimental platform;
- Analyze and compare commercial inverters output current.

1.4 Document structure

This work is divided into 7 chapters to describe what was done through the development of it. The first chapter presents an introduction to renewable energies (RE) and its influence on grid quality and the requirements for grid interconnection. Chapter 2 brings a review of current control methods and output filters for inverters.

The chosen power structure and filter design methods are presented in Chapter 3. Chapter 4 is focused on simulation implemented and the results of the computational tests. Chapter 5 is dedicated to the experimental platform and test results. The analysis and discussion over the results are presented in Chapter 6 and Chapter 7 is dedicated to the conclusion and future works suggestions.

Chapter 2

Current improvement techniques

2.1 AC-DC converter control

2.1.1 PI in the natural frame

The Proportional-Integrative-Derivative (PID) controller is applied to more than half of industrial controllers, due to its simple tuning methods and good applicability even when the mathematical model of the system is unknown [14]. The structure of a PID controller is presented in Figure 2.1.

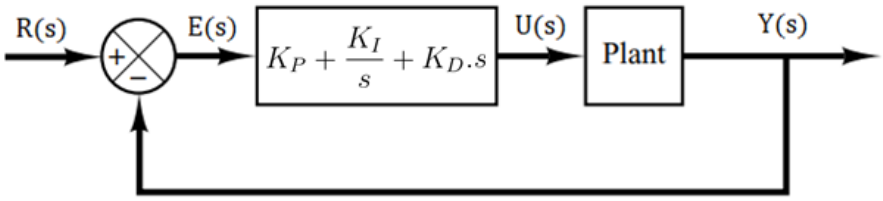

Figure 2.1: Structure of a PID controller, adapted from [14].

Where K_p, K_i and K_d are the proportional, integral and derivative gains, respectively. However, for this work and by literature analysis, the derivative part is not necessary and will not be implemented.

When the variables of a three-phase system are controlled or manipulated as sinusoidal values, without any transformation, they are in the natural (or *abc*) frame. The PI controller has a good and fast response in most of the linear systems. It can be applied to control variables in the natural frame. However, the zero steady-state error condition is limited to dc values of reference [10].

The PI controller in the natural frame is enough to be applied in simple applications that do not require that the current follows precisely the reference and with fewer restrictions.

Nevertheless, when using sinusoidal references, the PI controller will always have a steady-state error. Thus, in some cases, more robust and precise alternatives are needed to fulfill legal requirements and provide good current quality.

2.1.2 PI in the synchronous frame

To use the PI controller to control alternate current with low steady-state error, it is possible to employ frame transformations and use DC values as control variables. The synchronous frame, also called dq frame, is a frame that rotates in the same frequency as the natural frequency of the abc frame. Since this frame has the same angular speed of the grid voltage, the sinusoidal variables are transformed to dc values, and then the PI controller can be used to achieve a zero steady-state error.

To control single-phase currents with this technique, a virtual $\alpha\beta$ frame is created using a virtual current delayed by 90 degrees of the real current. With Park transformation then is possible to control these variables as dc values in the dq frame [15]. One drawback of this solution is that the transformations mentioned above require computational power to perform, resulting in larger firmware and longer computing periods.

Knowing the phase angle (θ) of the wave and considering the output current as i_α, a second wave delayed 90 degrees (i_β) is generated to properly use Park transformation, as represented by:

$$\begin{bmatrix} i_d \\ i_q \end{bmatrix} = \begin{bmatrix} \cos\theta & \sin\theta \\ -\sin\theta & \cos\theta \end{bmatrix} \cdot \begin{bmatrix} i_\alpha \\ i_\beta \end{bmatrix} \tag{2.1}$$

Using grid voltage and current in the rotating reference frame (dq) it is possible to use pq theory to individually control active and reactive power injection [16]. If θ is chosen properly that the quadrature component of voltage is null, the powers can be calculated as:

$$p = \frac{1}{2} \cdot v_d \cdot i_d \tag{2.2}$$

$$q = -\frac{1}{2} \cdot v_d \cdot i_q \tag{2.3}$$

By the equations (2.2) and (2.3) the current references are defined by:

$$i_d^* = \frac{2 \cdot p}{v_d} \tag{2.4}$$

$$i_q^* = -\frac{2 \cdot q}{v_d} \tag{2.5}$$

Figure 2.2 shows the block diagram of implemented control using synchronous frame control and *pq* theory to control inverter output, as presented in [17].

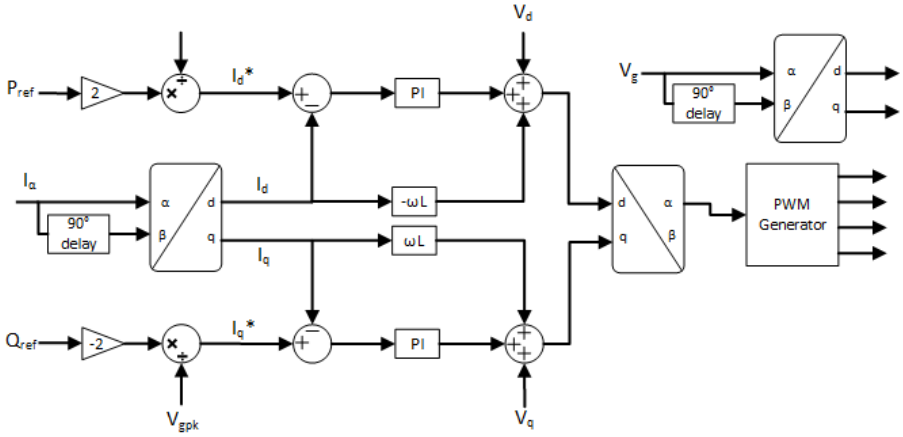

Figure 2.2: Block diagram of control using synchronous frame [17].

2.1.3 Proportional resonant controller

Alternatively to the PI controller, there is the proportional resonant (PR) controller. This controller is similar to the PI controller, but instead of an infinite dc gain, it has an infinite gain at a chosen resonant frequency (ω). With this feature, it is not necessary to use frame transformations to achieve zero steady-state error when controlling ac variables.

With the PR controller, it is also possible to have multiple controllers at different frequencies to provide harmonic correction of the output current or even use the inverter as an active filter for harmonics. The equation of a PR controller is given by:

$$C_{PR}(s) = K_P + \frac{2 \cdot K_I \cdot s}{s^2 + \omega^2} \tag{2.6}$$

The harmonic compensator (HC) is defined by:

$$C_{HC}(s) = \sum_{h=3,5,7,..} \frac{2 \cdot K_{ih} \cdot s}{s^2 + (h \cdot \omega)^2} \tag{2.7}$$

However, infinite gain can lead to system stability problems. To avoid that, a cut-off frequency (ω_c) is introduced to equations (2.6) and (2.7). This results in a more stable system and a widened bandwidth gain, which is good for systems where there is some flotation on the frequency ($\sim$1% of rated frequency), for example, on grid-connected applications [18]. With this, the equations can be written as:

$$C_{PR}(s) = K_P + \frac{2 \cdot K_I \cdot \omega_c \cdot s}{s^2 + 2 \cdot \omega_c \cdot s + \omega^2} \tag{2.8}$$

$$C_{HC}(s) = \sum_{h=3,5,7,..} \frac{2 \cdot K_{ih} \cdot \omega_c \cdot s}{s^2 + 2 \cdot \omega_c \cdot s + (h \cdot \omega)^2} \tag{2.9}$$

The bode plot for both resonant controller with infinite gain and with limited gain are presented on Figure 2.3. For the plots the gains used were $K_P = 1$, $K_I = 20$, $\omega = 314 rad/s$ and $\omega_c = 10 rad/s$.

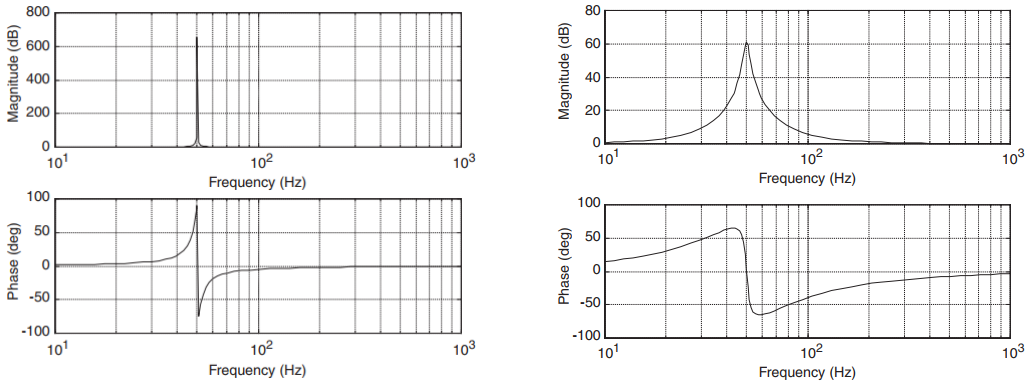

(a) Infinite gain (b) Limited gain

Figure 2.3: Bode plots for PR controller [18].

2.1.4 Deadbeat controller

Predictive controllers are the controllers that estimate the output of the control signal using a system model to achieve a specified result. The deadbeat controller is a predictive type of controller applied in output inverter current control [19]. It is necessary to know the inverter and output filter model, which can be obtained by the circuit analysis or system identification techniques.

With the transfer function that relates output current and inverter output voltage and, hence, the inverter duty cycle, the controller calculates at each switching period the duty cycle value for the next switching period using the model, references, and measured values. Since this controller relies on the model, variations of system parameters affect controller response, being a major drawback [20].

2.1.5 Repetitive controller

The repetitive controller is a type of simple learning controller. It uses the error from previous periods to determine the output. This controller is very useful to control periodic references, since it has a time delay in its structure. With this time delay, any periodic signal can be generated providing a good initial function. Then, the internal model principle is respected and a zero steady-state error can be achieved [21].

To ensure system stability, it is usual to have one or two filters along with the repetitive control structure. These filters can have several different topologies and can be used in different points of the structure. One application, proposed in [22], is presented in Figure 2.4. Where $Q(s)$ and $M(s)$ are the filters, and L is the period of the reference.

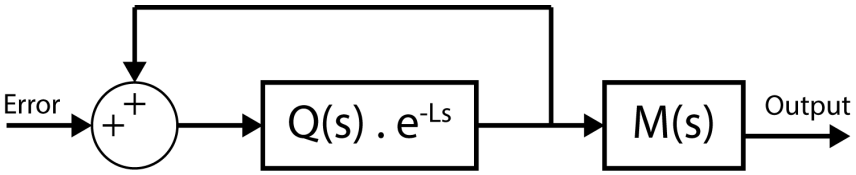

Figure 2.4: Repetitive structure, adapted from [22].

2.2 Output filter

The inverters used in RE systems use pulse width modulation (PWM) switching as a technique to generate its output. This modulation results in high interference of harmonics around the switching frequency. Low-pass filters are a well-known solution to filter the harmonics and improve power quality. There are several filter configurations proposed in the literature. The most common are the L filter, LC filter, and LCL filter, presented in Figure 2.5, where the controlled voltage source (V_{ab}) represents the output of the VSI and the AC source (V_g) represents the grid voltage. In the following sections, these three filter configurations will be discussed and analyzed.

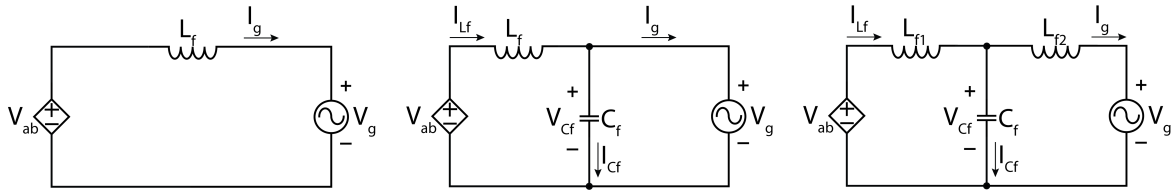

(a) L Filter (b) LC Filter (c) LCL Filter

Figure 2.5: Filter topologies, adapted from [23].

2.2.1 L Filter

The L filter consists of a single inductor connected between inverter output and grid, it was used in older studies to reduce the ripple output in inverters. However, to fulfill the requirements of the regulations demands high values of inductance, resulting in poor system dynamics due to a high voltage drop and increasing weight and size of the magnetic element. To mitigate this problem, a higher switching frequency can be used. Higher the operation frequency, the smaller the magnetic elements have to be. However, other components of the system may limit the frequency value that can be used, components like power switches, and the PWM generator. [24].

2.2.2 LC Filter

The LC filter consists of a series inductor and a capacitor in parallel connection with the grid. The capacitor provides a low impedance path for the higher frequency harmonics, being more recommended to meet the requirements of the standards. Nevertheless, this configuration requires more attention to be designed, since the capacitor value has to be lower enough to does not cause high inrush currents and does not consume much of reactive power [23]. The detailed structure of an LC filter is presented in Figure 2.5b a controlled voltage source was used to represent the VSI output to simplify the analysis. From the presented circuit it is possible to find the transfer function of the filter, shown in Equation (2.10), and with that, the bode plot of the filter is depicted in Figure 2.6.

$$\frac{V_c(s)}{V_o(s)} = \frac{1}{L_f \cdot C_f \cdot s^2 + 1} \tag{2.10}$$

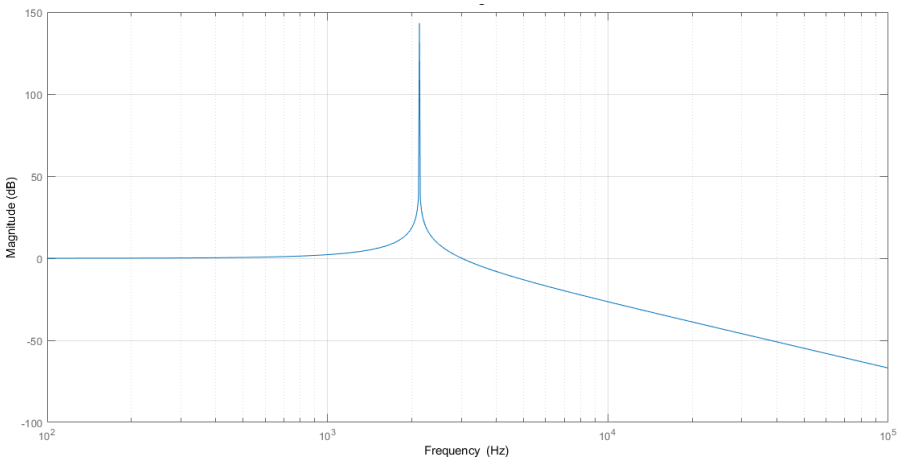

Figure 2.6: Bode plot for LC fitler, adapted from [23].

2.2.3 LCL Filter

Another type of filter is the LCL filter, which is similar to the LC filter, but with one more inductor between the shunt capacitor and the grid. This configuration results in a third-order filter, requiring smaller passive components to reduce harmonics and ripple of high frequencies compared to the LC filter. Nonetheless, such a complex filter results in a more complex control system design, causing resonance problems on specific frequencies [25]. This resonance problem can be avoided using damping strategies, that can be active or passive. The passive damping usually is implemented by adding resistors in series or parallel to the filter to avoid low impedance on some frequencies, but this implies lower efficiency due to power lost on the resistors. Active damping is a solution with no power loss that changes the control structure to improve system robustness, there are many methods to perform that, but usually requires more sensors and precise parameters setting for the control [23]. Therefore, due to its complexity, the LCL filter will not be more discussed in this work.

Chapter 3

Power Topology

The power topology adopted for this work was already tested and used in several works from the Electro Mechatronics Systems Laboratory (LSE) of IPB [26]–[28]. It is a robust and simple structure that can be used in different applications. It consists of three IGBT legs, where one is responsible for the DC-DC stage, acting as a boost or buck converter according to the application and the other two legs make an h-bridge inverter. Figure 3.1 presents the power structure adopted and Table 3.1 shows the parameters for the chosen topology.

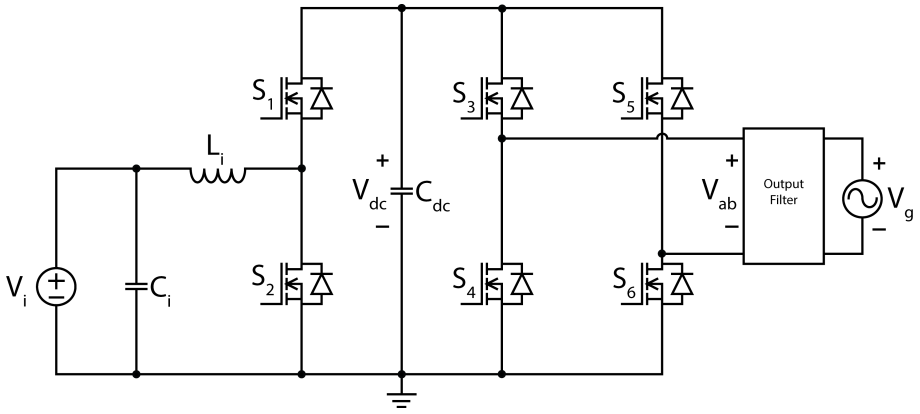

Figure 3.1: Power structure adopted

Parameter	Value
V_i	$96V$ (8x$12V$ Batteries)
C_i	$0.5\mu F$
L_i	$12mH$
C_{DC}	$0.5\mu F$
V_{DC}	$400V$
V_g	$230V_{rms}$
f_g	$50Hz$
f_s	$10kHz$

Table 3.1: Experimental platform parameters

3.1 DC-DC converter

The input of the DC-DC converter can be a photovoltaic system, a battery bank, or even AC generators with a rectification stage from wind or hydro turbines. When using a battery as input, the power flow can be bidirectional to allow battery charging as well.

When charging the batteries, the power flows from the grid to the batteries, and the converter behaves as a buck converter (S_1 switching and S_2 off). If the converter are injecting power to the grid, it behaves as a boost converter (S_1 off and S_2 switching). When operating as a boost it controls the DC link voltage and when operating as a buck it controls battery voltage and current.

The DC-DC converter can control the DC link voltage or the power requested from the batteries. If controlling the power, then the VSI would be responsible for controlling DC link voltage. However, since this work is focused on inverter behavior, the DC-DC stage was used only to maintain the DC link voltage at the desired value to supply the grid current and will not be deeply discussed.

3.2 DC-AC converter

Between the DC link and the low-pass filter there is an h-bridge inverter (Figure 3.2). It can work as an active rectifier when charging the batteries, controlling grid current (obtaining unity power factor), or as a voltage source inverter when supplying power to the grid. The converter is bidirectional and can drain current from the grid with a unity power factor or inject a sinusoidal current to the grid.

3.2.1 Output voltage model

Considering a full-bridge inverter, the determination of the output voltage (V_{ab}) behavior is important to properly control the output current.

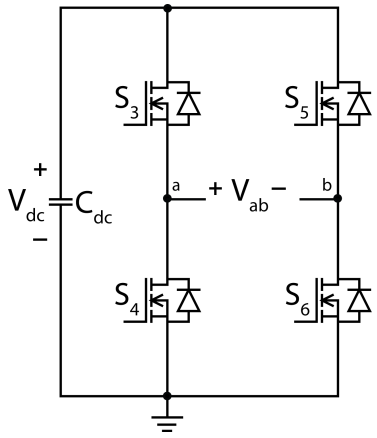

Figure 3.2: Full-bridge inverter

A 3-level PWM switching was used on this work, which means that the output voltage has three different values: $+V_{dc}$, $-V_{dc}$, and zero. The PWM signals of a switching period and the output voltage of the inverter are shown in Figure 3.3. The analysis was made for the positive cycle of the grid voltage, but for the negative cycle, the operation is similar.

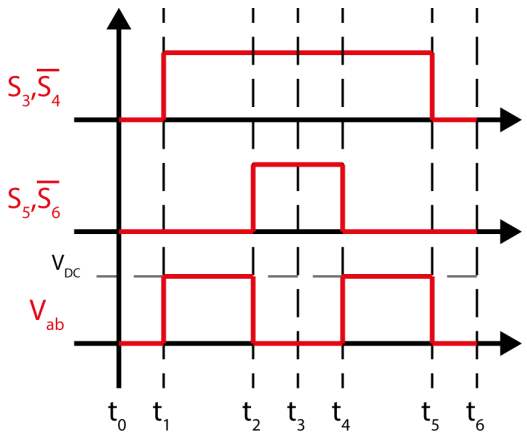

Figure 3.3: PWMs and output voltage of a VSI

The instant t_6 is equal to the switching period (T_s), and $t_3 = T_s/2$, it is also known that $t_5 - t_1 = D \cdot T_s$ and $t_4 - t_2 = (1 - D) \cdot T_s$, with this the time interval from t_1 to t_2 can be written as $(2 \cdot D - 1) \cdot T_s/2$, where D is the inverter duty cycle. With this time interval it is possible to determine the average value of the output voltage in a switching period, and the relation between V_{ab} and V_{dc} is shown in (3.1).

$$V_{ab} = 2 \cdot \frac{V_{dc} \cdot (2 \cdot D - 1) \cdot T_s/2}{T_s}$$

$$V_{ab} = V_{dc} \cdot (2.D - 1)$$

$$\frac{V_{ab}}{V_{dc}} = (2 \cdot D - 1) \tag{3.1}$$

The duty cycle (D) can be written as:

$$D = \frac{\frac{V_{ab}}{V_{dc}} + 1}{2}$$

Considering that V_{ab} is equal to grid voltage (V_g):

$$D(\omega t) = \frac{m \cdot sin(\omega t) + 1}{2} \tag{3.2}$$

Where $m = V_{dc}/V_{pk}$, and V_{pk} is the grid peak voltage.

3.3 Output filter design

3.3.1 L Filter

The inductance value is usually determined to limit the output current ripple. Knowing the voltage across the inductor it is possible to calculate the minimum inductance to ensure that the current ripple does not surpass the maximum ripple determined. The voltage and current through the inductor are depicted in Figure 3.4.

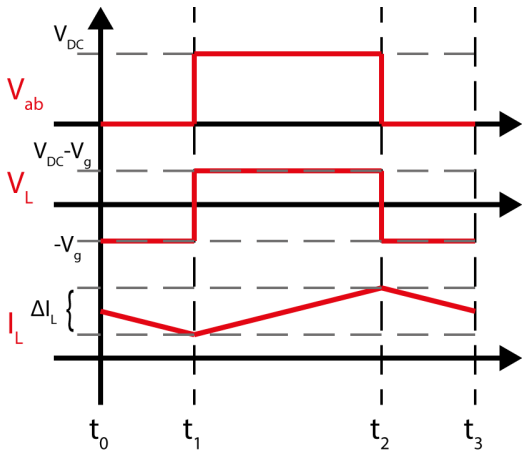

Figure 3.4: Voltage and current on the inductor

The current ripple is determined by the voltage across the inductor in the time interval between t_1 and t_2.

$$V_L = L \cdot \frac{di_L}{dt}$$

$$V_L = L \cdot \frac{\Delta i_L}{\Delta t}$$

$$V_{dc} - V_g = L \cdot \frac{\Delta i_L}{\frac{2 \cdot (2 \cdot D - 1)}{T_s}} \tag{3.3}$$

Replacing (3.2) in (3.3) and isolating Δi_L.

$$\Delta i_L(t) = \frac{T_s \cdot V_{pk}}{2 \cdot L} \cdot [sin(\omega t) - m \cdot sin^2(\omega t)] \tag{3.4}$$

$$L(t) = \frac{T_s \cdot V_{pk}}{2 \cdot \Delta i_L} \cdot [sin(\omega t) - m \cdot sin^2(\omega t)] \tag{3.5}$$

To determine the minimum possible value for the inductor it is necessary to find the time where the function (3.5) is minimum, and for that is used the derivative.

$$\frac{dL}{dt} = 0 \rightarrow t_{L,min}$$

$$\frac{T_s \cdot V_{pk}}{2 \cdot \Delta i_L} \cdot [cos(\omega \cdot t_{L,min}) - 2 \cdot m \cdot sin(\omega \cdot t_{L,min}) \cdot cos(\omega \cdot t_{L,min})] = 0$$

$$1 - 2 \cdot m \cdot sin(\omega \cdot t_{L,min}) = 0$$

$$t_{L,min} = \frac{asin(\frac{1}{2 \cdot m})}{\omega} \tag{3.6}$$

Replacing (3.6) in (3.5) it is possible to determine the minimum inductance value to limit the current ripple in a desired value, represented in (3.7).

$$L_{min} = \frac{T_s \cdot V_{pk}}{2 \cdot \Delta i_L} \cdot [sin(\omega t_{L,min}) - m \cdot sin^2(\omega t_{L,min})] \tag{3.7}$$

3.3.2 LC Filter

By the filter transfer function (Eq. (2.10)), it is possible to obtain the resonance frequency of the filter, presented on (3.8).

$$f_r = \frac{1}{2 \cdot \pi \cdot \sqrt{L_f \cdot C_f}} \tag{3.8}$$

To avoid resonance between the filter and the inverter the resonant frequency of the filter should be less than 0,5 of the switching frequency (f_s). In order to prevent that the filter affects at the fundamental grid frequency (f_g), f_r should be at least 10 times greater than f_g [23].

$$10 \cdot f_g < f_r < 0.5 \cdot f_s \tag{3.9}$$

The inductor value should be higher enough to prevent high current ripple, as well as in the L filter, and Eq. (3.7) can also be used to the LC filter. However, the inductance must have a lower value to avoid high voltage drop (V_L) between inverter output and grid connection point, in this case a voltage drop of 10% is selected [29].

$$V_L = X_L.I_L < 0.1 \cdot V_g$$

$$V_L = 2 \cdot \pi \cdot f_g \cdot L \cdot \frac{P_N}{V_g} < 0.1 \cdot V_g$$

$$L_{max} = \frac{0.1 \cdot V_g^2}{2 \cdot \pi \cdot f_g \cdot P_N} \tag{3.10}$$

Where P_N is the rated inverter power, f_g is the grid frequency and V_g is the grid rms voltage.

Higher capacitances have better filtering, nevertheless, it is important to limit its value to avoid high reactive power consumption from the filter capacitance. Usually, the capacitor reactive power is limited to 5% of the inverter rated power [23].

$$P_C = \frac{V_g^2}{X_C} < 0.05 \cdot P_N$$

$$V_g^2 \cdot 2 \cdot \pi \cdot f_g \cdot C < 0.05 \cdot P_N$$

$$C_{max} = \frac{0.05 \cdot P_N}{V_g^2 \cdot 2 \cdot \pi \cdot f_g} \tag{3.11}$$

The inductance and capacitance value must be selected respecting the limits determined by (3.7), (3.9),(3.10) and (3.11).

3.4 DC-DC converter control

The first stage of the converter is responsible for elevating the input voltage to an appropriate value so the inverter can inject power to the grid. The control consists of two loops, as depicted in Figure 3.5, the first one controls DC bus voltage, comparing the actual value with the reference and passing the error through a PI controller. The second loop controls the battery current, using the output of the first PI as a reference, and comparing it to the actual value, the error goes through another PI that generates the duty cycle value for the first stage switch.

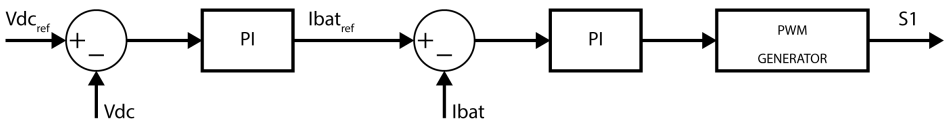

Figure 3.5: Control loop for first stage with battery on input

If the input was a photovoltaic system instead of a battery, the control of the first stage (DC-DC converter) is responsible for the maximum power point tracking (MPPT). Adopting a perturb and observe method, the input voltage reference is changed until the maximum power point is found. This voltage reference is compared to the actual value and the error pass through a PI controller that generates the duty cycle value, as shown in Figure 3.6.

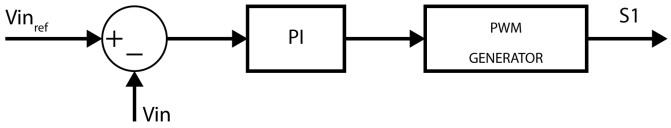

Figure 3.6: Control loop for first stage with PV on input

Since the tests were made using batteries as input, the implemented control structure was the one depicted in Figure 3.5. The gains for the controller are presented in Table 3.2.

Parameter	**Value**
Kp_{Vdc}	0.35
Ki_{Vdc}	8.0
Kp_{Ib}	0.05
Ki_{Ib}	7.0

Table 3.2: Gains for the DC-DC controller

Chapter 4

Simulation Tests

To verify if the control algorithms and power structure adopted will work well in the proposed conditions, it is important to test it in a simulation environment. So, a MATLAB/Simulink model of the system was used to validate it before the experimental tests.

4.1 Simulation model

4.1.1 Power structure

The power structure already described in Chapter 3 (Figure 3.1) was designed on Simulink using the Specialized Power Systems library of Simscape, presented in Figure 4.1. A step time of 2 μs was chosen, however, since the experimental system will have a switching frequency of 10 kHz, this frequency was chosen as the sampling frequency of the control algorithm.

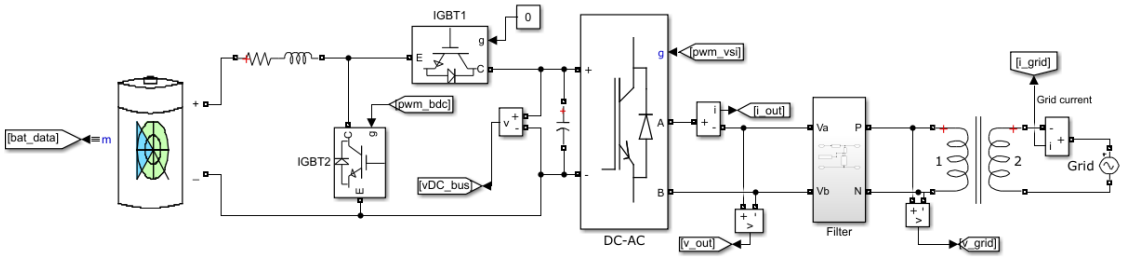

Figure 4.1: Power structure implemented on Simulink

4.1.2 PI Controller

As described in Chapter 2, several PI controllers were used in the control of the DC-DC stage and also in the synchronous frame control of the DC-AC stage. The parallel

implementation was chosen, where the proportional and integral actions are summed. Since the simulation model should be as close as possible to the experimental platform, the control algorithm was implemented on the discrete-time.

There are three common discrete approximations to the continuous integrator: Forward Euler, Backward Euler, and Tustin.

$$\text{Forward Euler:} \qquad \frac{1}{s} = T_s \cdot \frac{1}{z-1} \tag{4.1}$$

$$\text{Backward Euler:} \qquad \frac{1}{s} = T_s \cdot \frac{z}{z-1} \tag{4.2}$$

$$\text{Tustin:} \qquad \frac{1}{s} = \frac{T_s}{2} \cdot \frac{z-1}{z+1} \tag{4.3}$$

Where T_s is the sampling time of the discrete system.

For the PI controllers, it was chosen the Forward Euler approximation. Figure 4.2 presents the PI block implemented.

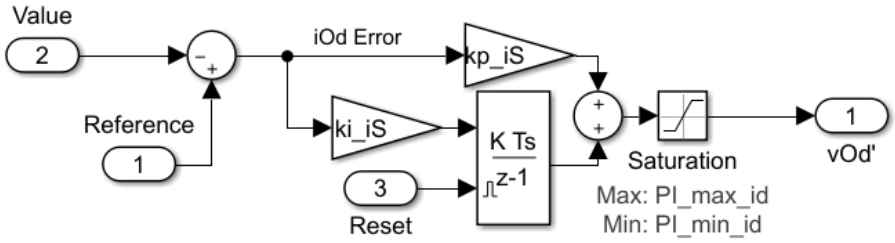

Figure 4.2: PI controller implemented in Simulink

4.1.3 Frame transformation

The reference frame transformations were applied according to Equation (2.1), to the $\alpha\beta - dq$ transformation and using the inverse to the $dq - \alpha\beta$. The phase angle (θ) was acquired using a phase locked loop algorithm. Figures 4.3 and 4.4 presents the transformations blocks.

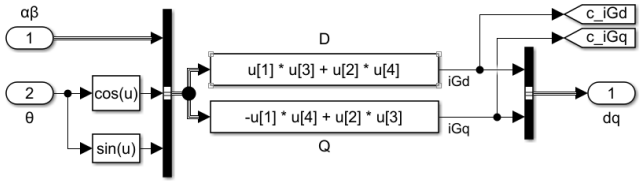

Figure 4.3: $\alpha\beta - dq$ transformation block

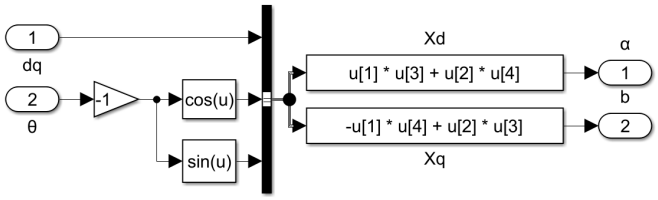

Figure 4.4: $dq - \alpha\beta$ transformation block

4.1.4 Phase-locked loop model

The Phase-locked loop (PLL) is responsible for determining the phase angle (θ) of an input signal, in this case, the grid voltage. This variable is important to properly use the frame transformations mentioned before and also to assure that the injected current is in phase with the grid voltage. The PLL was implemented as in Figure 4.5 and this structure was based on the PLL proposed in [30].

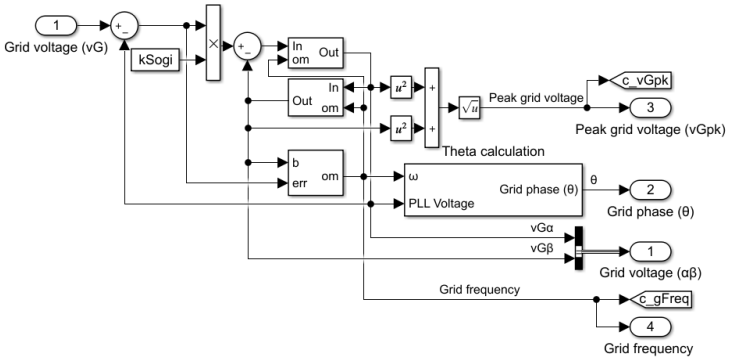

Figure 4.5: PLL block

4.1.5 Proportional resonant control model

To implement the PR controller in Simulink it was used the block diagram of the resonant link decomposed on two interlinked integrators (Figure 4.6), as presented in [18]. However, since the platform is based on discrete-time it is important to represent the continuous integrators in a discrete equivalent.

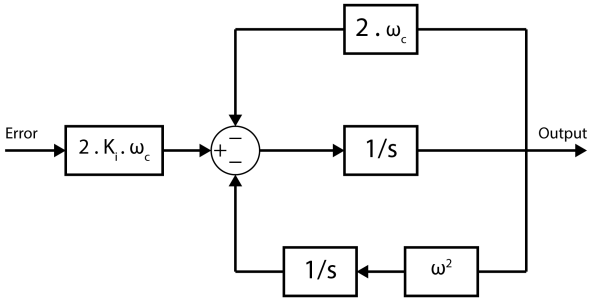

Figure 4.6: Representation of resonant link, adapted from [31]

To avoid algebraic loops, the integrator on the direct loop is represented with a Forward Euler. Since this approximation deviate from the -90 degrees phase on higher frequencies, a Backward Euler representation is used on the feedback loop. In this way it can compensate the deviation from the first integrator [32]. With this, the block diagram of the implemented resonant block in Simulink is presented in Figure 4.7.

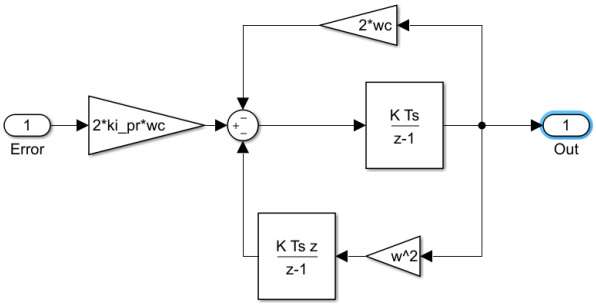

Figure 4.7: Resonant block in simulink

The resonant action in the fundamental frequency is summed with the proportional and the harmonic compensators actions, composing the action of the proportional resonant controller.

4.2 Results

With the presented Simulink simulation 4.1, some tests were made to verify the system behavior and if it was stable. The first test consisted of the comparison between the synchronous frame control and the PR controller. It was also tested PR with harmonic compensation of the third, fifth, seventh, and ninth harmonics. The controller comparison was made using an L filter as an output filter, after that, tests with an LC filter on the output were done.

Likewise, as in the experimental platform, which will be further presented, the input inductor selected was with the value of $12mH$, the DC link capacitance was of $1000\mu F$ and a battery block with a nominal voltage of $96V$ and state of charge of 98% was used.

4.2.1 Comparison between PR and synchronous frame

To compare the performance of the controllers, simulations with four different references of power (P_{ref}) were made. Figure 4.8 presents the result of the simulation with $P_{ref} = 1000W$, Figure 4.9 shows the result to $P_{ref} = 750W$, for a power reference of 500 W the result is presented in Figure 4.10 and Figure 4.11 presents the simulation with $P_{ref} = 250W$.

The parameters used for the simulation were the same as the power structure presented in Chapter 3. On the output filter, an L filter with $L_f = 5.6mH$ was chosen, and the gains for the inverter controller are presented in Table 4.1, where Kp_{dq} and Ki_{dq} are the proportional and integral gain for the synchronous controller, Kp_{PR} and Ki_{PR} are the proportional and resonant gains for the PR controller, and Ki_{HC} is the gain for the harmonic compensators.

Gain	Kp_{dq}	Ki_{dq}	Kp_{PR}	Ki_{PR}	Ki_{HC}
Value	20	1000	25	750	750

Table 4.1: Gains for the inverter current controllers

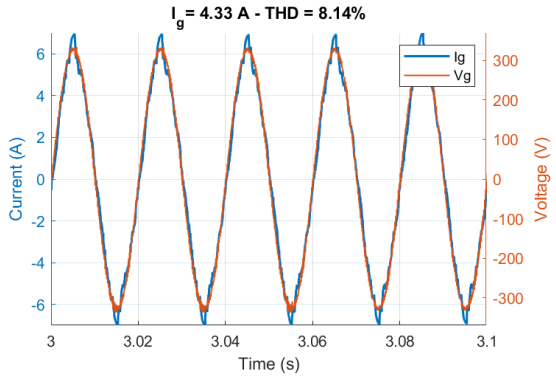

(a) Synchronous controller

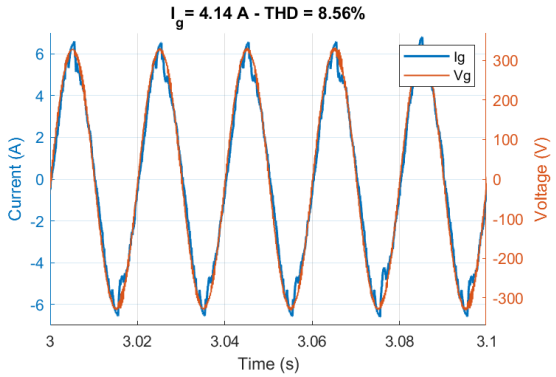

(b) PR Controller

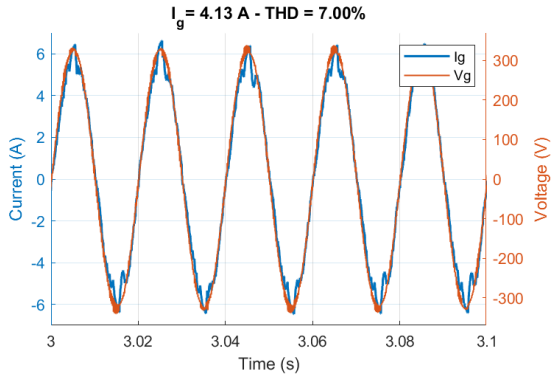

(c) PR + 3 HC

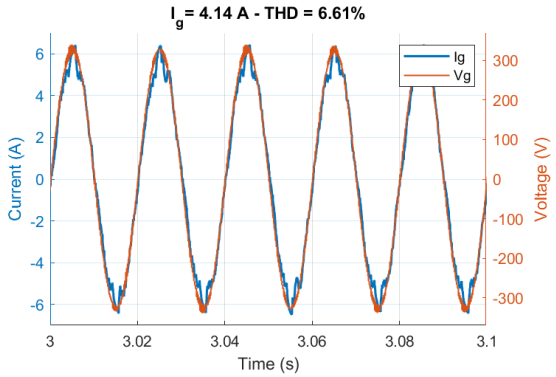

(d) PR + 3HC + 5HC

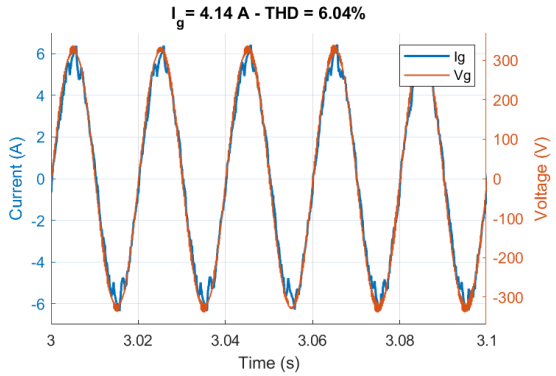

(e) PR + 3 HC + 5HC + 7HC

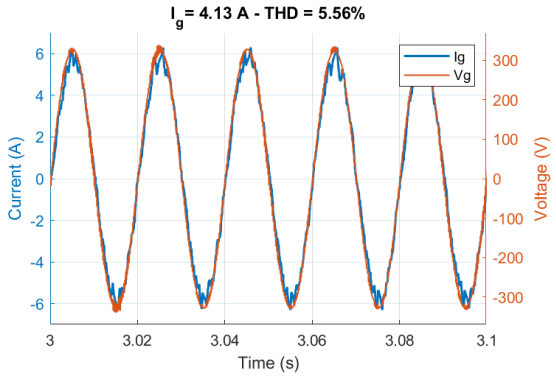

(f) PR + 3 HC + 5HC + 7HC + 9HC

Figure 4.8: Test with reference power of 1000 W

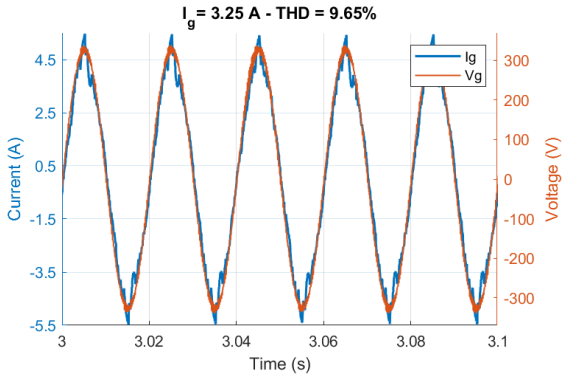

(a) Synchronous controller

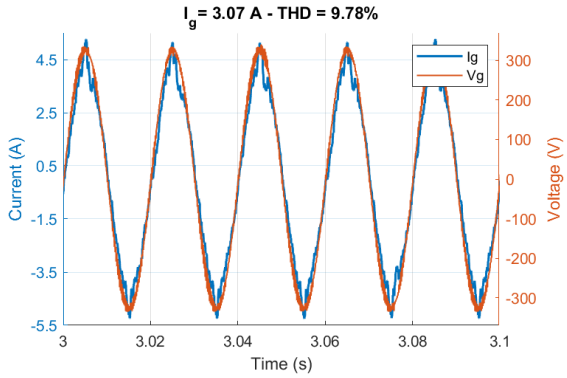

(b) PR Controller

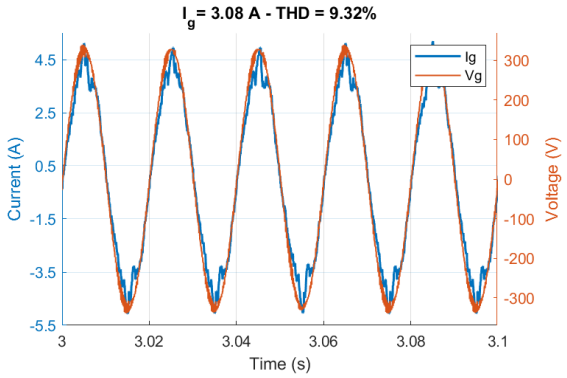

(c) PR + 3 HC

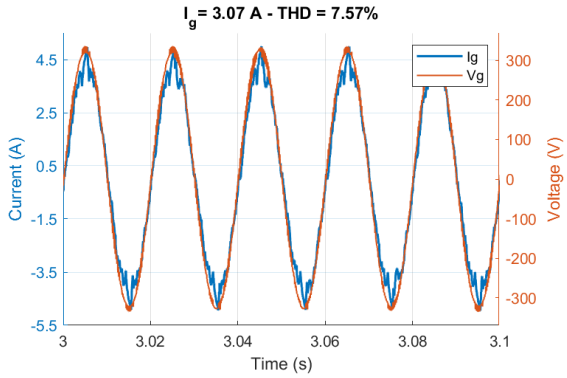

(d) PR + 3HC + 5HC

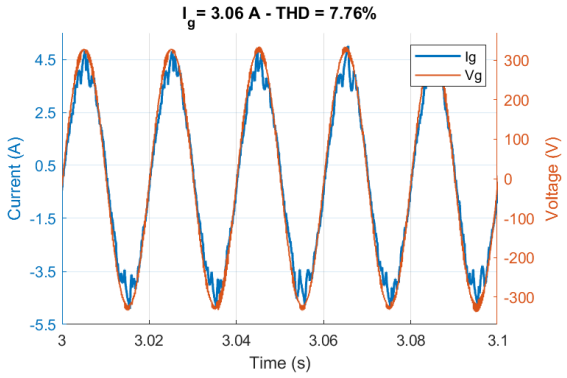

(e) PR + 3 HC + 5HC + 7HC

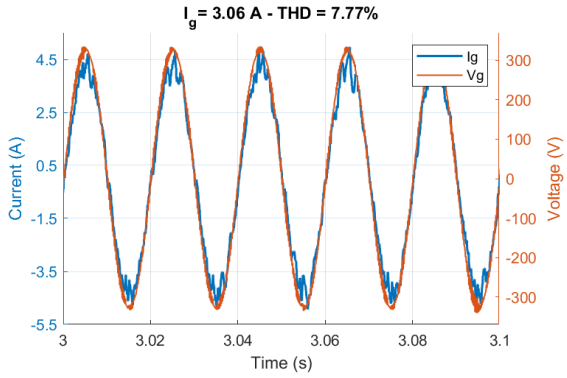

(f) PR + 3 HC + 5HC + 7HC + 9HC

Figure 4.9: Test with reference power of 750 W

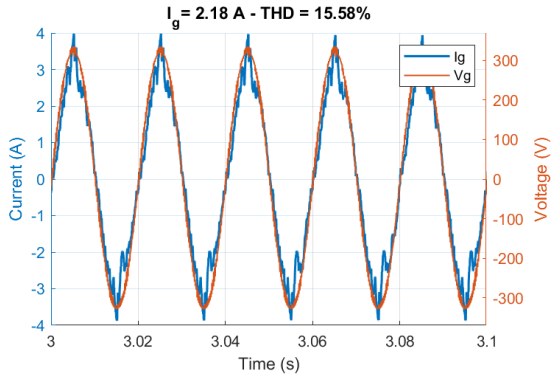

(a) Synchronous controller

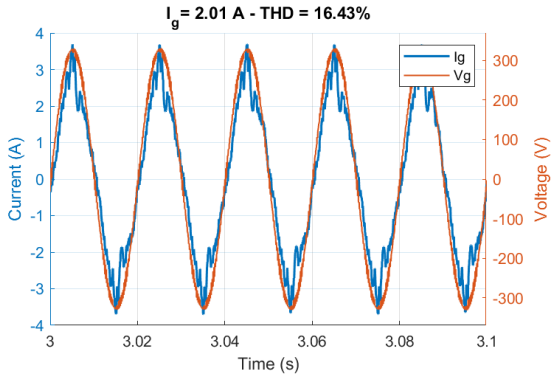

(b) PR Controller

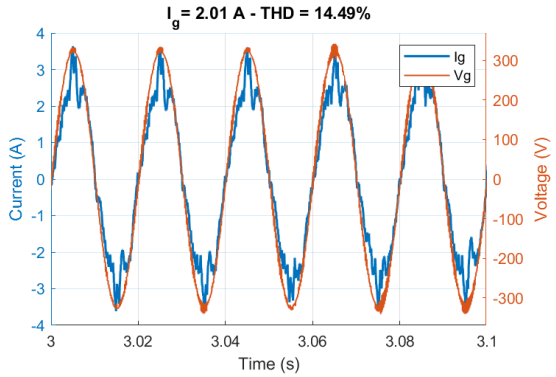

(c) PR + 3 HC

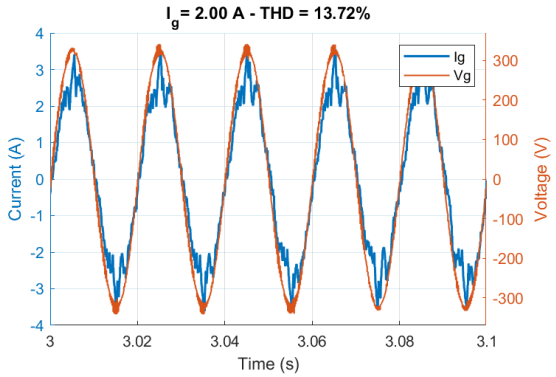

(d) PR + 3HC + 5HC

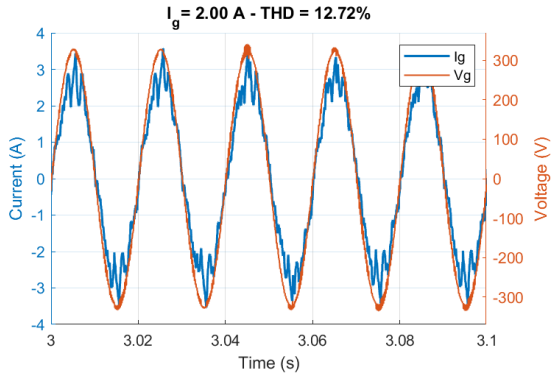

(e) PR + 3 HC + 5HC + 7HC

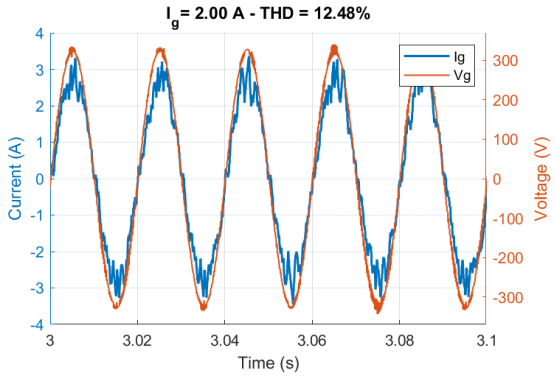

(f) PR + 3 HC + 5HC + 7HC + 9HC

Figure 4.10: Test with reference power of 500 W

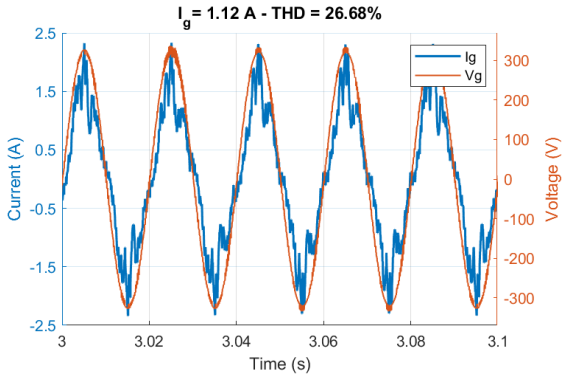

(a) Synchronous controller

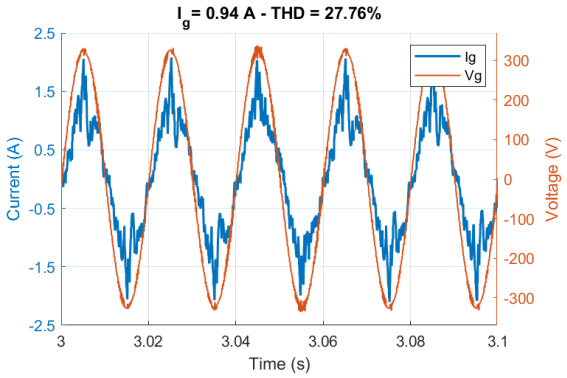

(b) PR Controller

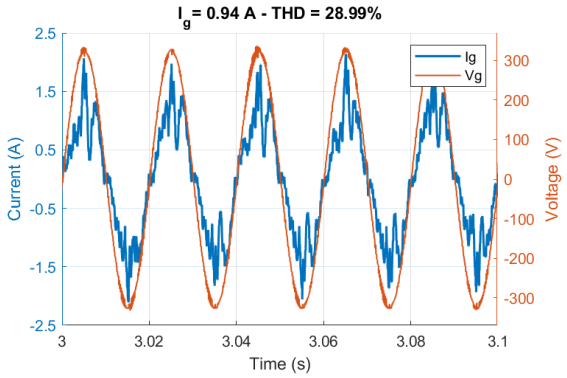

(c) PR + 3 HC

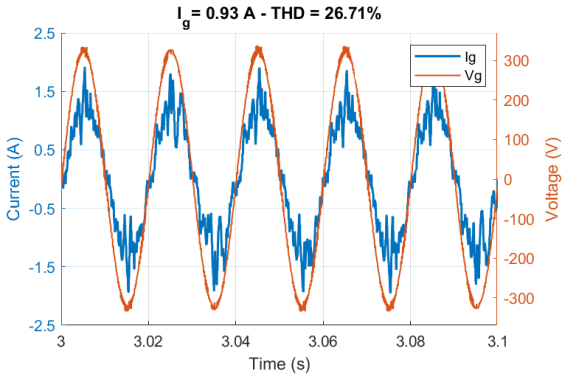

(d) PR + 3HC + 5HC

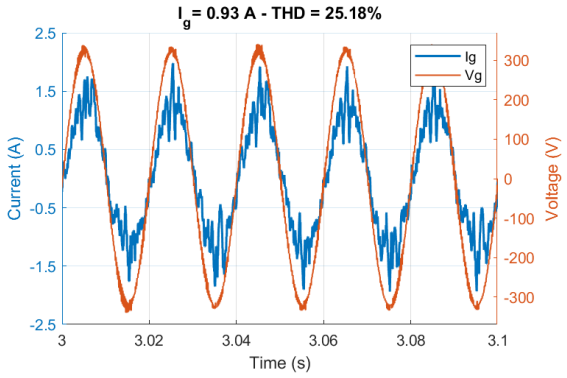

(e) PR + 3 HC + 5HC + 7HC

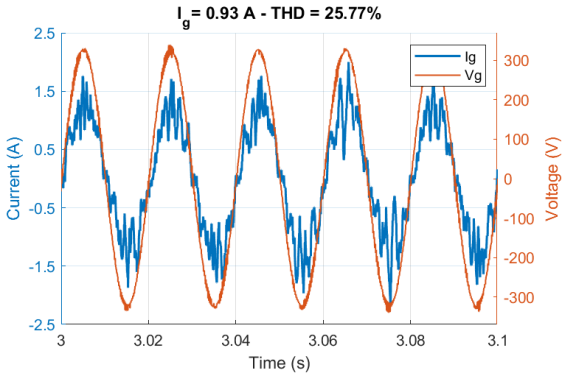

(f) PR + 3 HC + 5HC + 7HC + 9HC

Figure 4.11: Test with reference power of 250 W

4.2.2 Tests with LC filter

To investigate the influence of an LC filter on current quality, two values of the capacitor were tested as C_f: $1\mu F$ and $4.7\mu F$. Four power references were tested: 1000 W, 750 W, 500 W, and 250 W. The controller gains were the same as presented in Table 4.1 when $C_f = 1\mu F$ and for $C_f = 4.7\mu F$ the used gains are presented on Table 4.2. The presented results are for the synchronous controller and PR controller with harmonic compensation from third to ninth harmonic.

Gain	Kp_{dq}	Ki_{dq}	Kp_{PR}	Ki_{PR}	Ki_{HC}
Value	10	1000	10	1000	1000

Table 4.2: Gains for the inverter current controllers

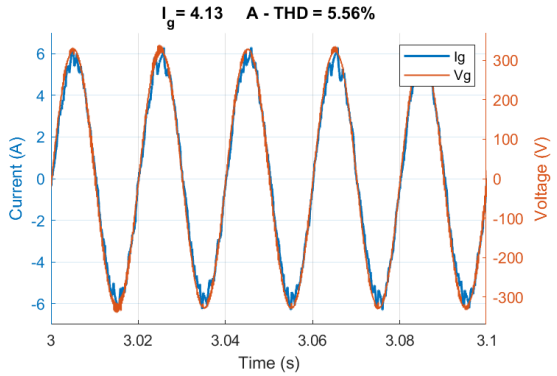

(a) PR Controller and $C_f = 1\mu F$

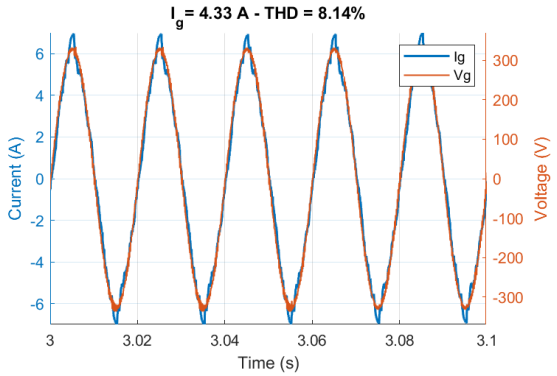

(b) Synchronous controller and $C_f = 1\mu F$

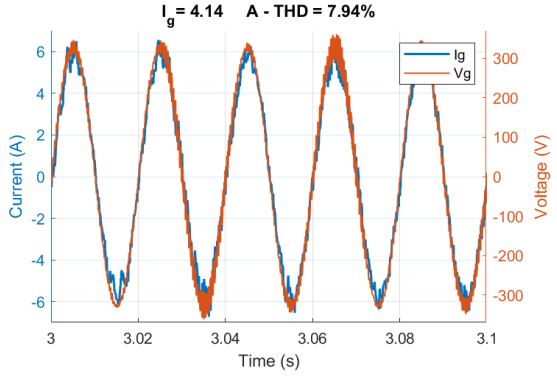

(c) PR Controller and $C_f = 4.7\mu F$

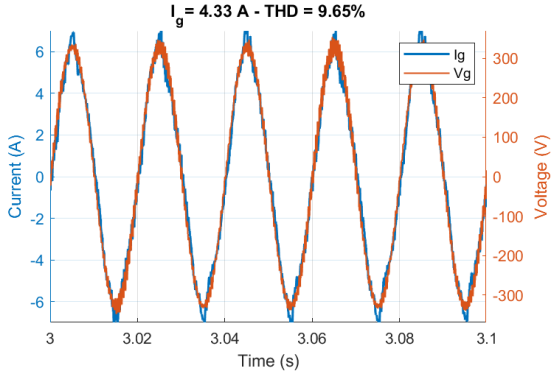

(d) Synchronous controller and $C_f = 4.7\mu F$

Figure 4.12: Test with LC filter and reference power of 1000 W

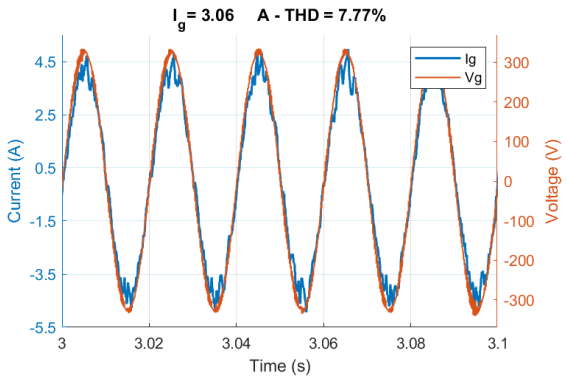

(a) PR Controller and $C_f = 1\mu F$

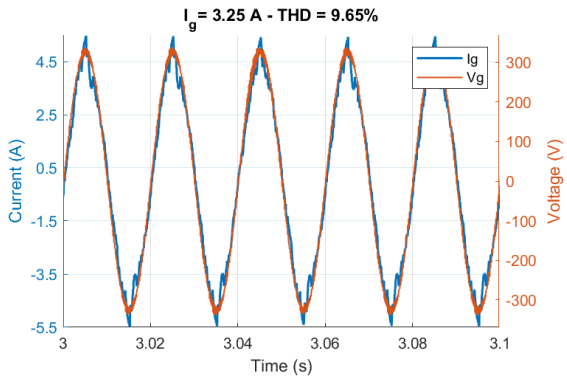

(b) Synchronous controller and $C_f = 1\mu F$

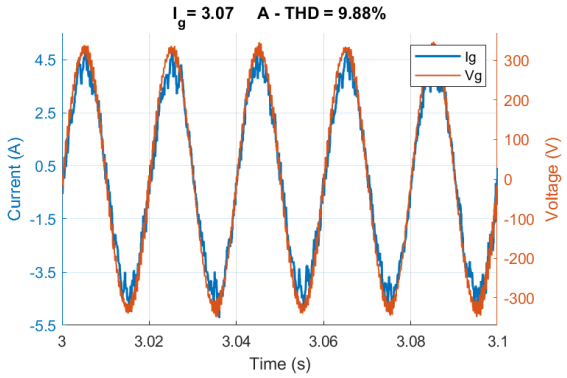

(c) PR Controller and $C_f = 4.7\mu F$

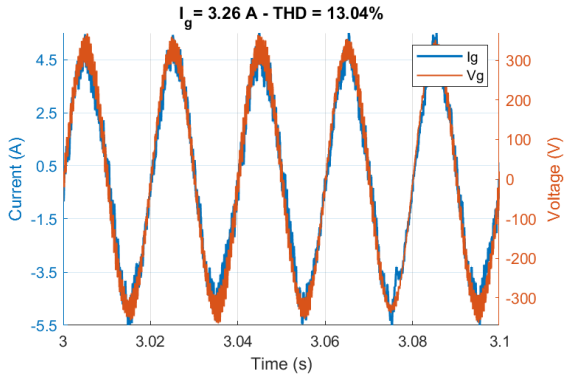

(d) Synchronous controller and $C_f = 4.7\mu F$

Figure 4.13: Test with LC filter and reference power of 750 W

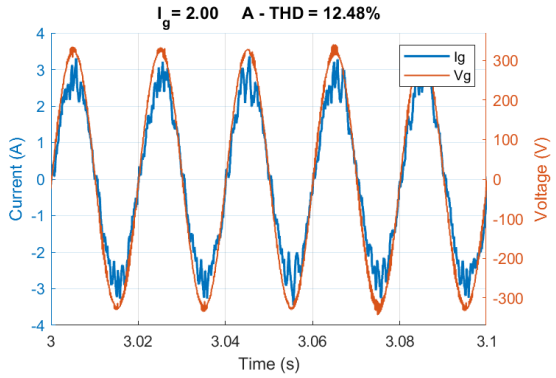

(a) PR Controller and $C_f = 1\mu F$

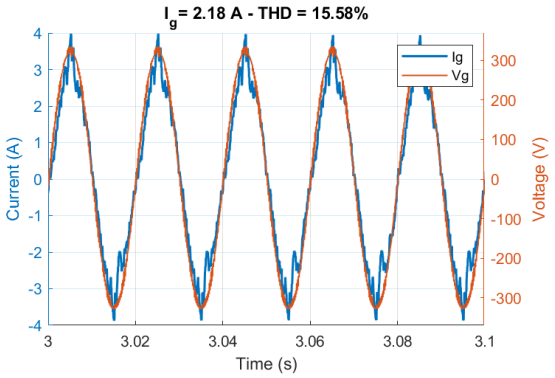

(b) Synchronous controller and $C_f = 1\mu F$

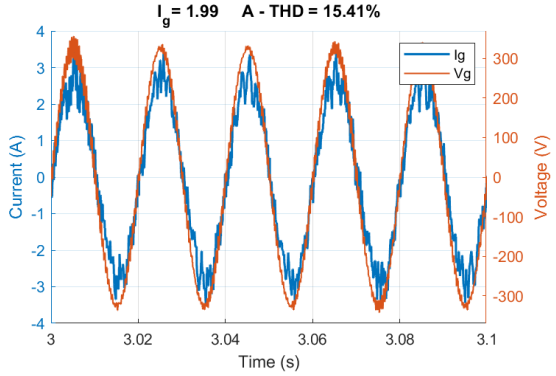

(c) PR Controller and $C_f = 4.7\mu F$

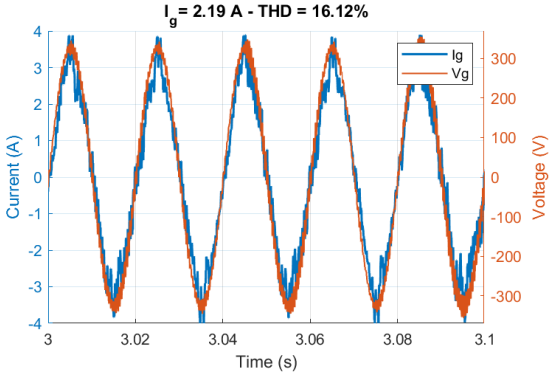

(d) Synchronous controller and $C_f = 4.7\mu F$

Figure 4.14: Test with LC filter and reference power of 500 W

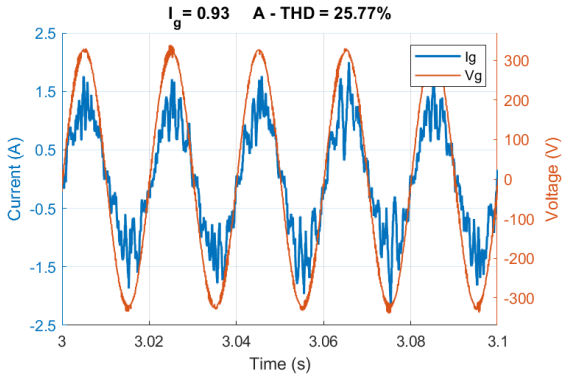

(a) PR Controller and $C_f = 1\mu F$

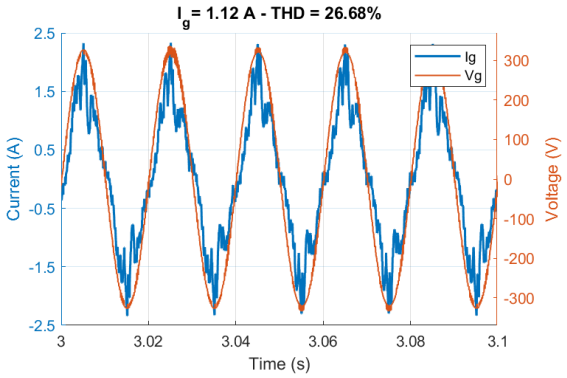

(b) Synchronous controller and $C_f = 1\mu F$

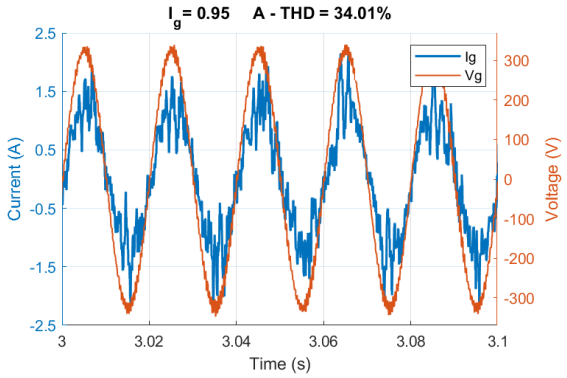

(c) PR Controller and $C_f = 4.7\mu F$

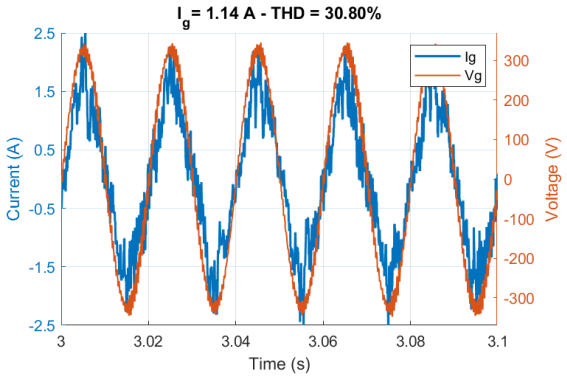

(d) Synchronous controller and $C_f = 4.7\mu F$

Figure 4.15: Test with LC filter and reference power of 250 W

Chapter 5

Experimental Tests

5.1 Experimental platform

For the experimental tests, an experimental platform previously developed on LSE was used. It consists of the power structure presented in Chapter 3 (Figure 3.1), a signal conditioning module, and a dSPACE DS1103 controller board and interface. The system is depicted in Figure 5.1.

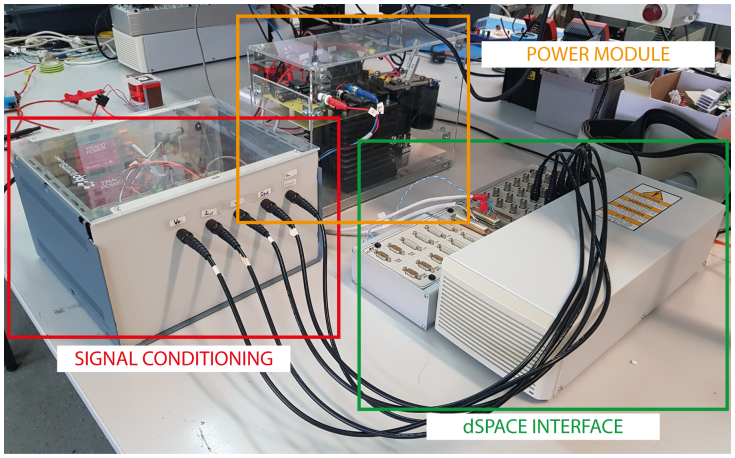

Figure 5.1: Experimental platform

5.1.1 Power structure

The power structure was implemented using the Powerex IGBT module PM75RLA120. This module is a three-phase IGBT inverter, with a rated current of 75 A and a rated voltage of 1200 V. For the DC link it was used four electrolytic capacitors of 1000 μF/400 V, arranged to compose 1000 μF/800 V capacitor. The input inductor (L_i) had a value of 12 mH and this value was selected to provide low current ripple when the converter is charging the batteries (DC-DC stage operating in buck mode). The BP7B interface, also from Powerex, is used to isolate the control signals sent from the control board to

the power switches, as well as adjusting the signal amplitude to properly drive the power switches. At the input, two polypropylene capacitors of $1\mu F$ were associated in series to compose the input capacitor, and eight 12 V Ultracell UCG 20-12 batteries in series composed the input source of 96 V.

5.1.2 dSPACE DS1103 Controller Board

The control of the structure was implemented using the DS1103 Controller Board from dSPACE, that is a simple and fast way to implement and prototype control structures in real-time. It provides a Real-Time Interface (RTI), and it is completely programmable with Simulink blocks.

Along with the DS1103, the ControlDesk software can be used to control and monitor the processor tasks in real-time. This is a software from dSPACE that works with the controller boards, where it is possible to watch and modify variables creating a functional environment to control and supervise system operation.

5.1.3 Signal conditioning module

To the control feedback signals, it was used LEM sensors to read current and voltage. Between sensors output and controller board input a signal conditioning stage was implemented, using an LTC1065 Low-Pass Filter to reduce noise and OP270 operational amplifiers to adjust signal amplitude to the controller board values (± 10 V).

Figure 5.2 shows the inside of the signal conditioning module. At the bottom, it is possible to see the TRACO power supplies of $\pm 15V$, $\pm 5V$, and $24V$, which supplies the signal board and BP7B interface of the power module. At the center of the image is the signal conditioning board, with the operational amplifiers and filter and under this board, not visible in the picture, are the voltage sensors.

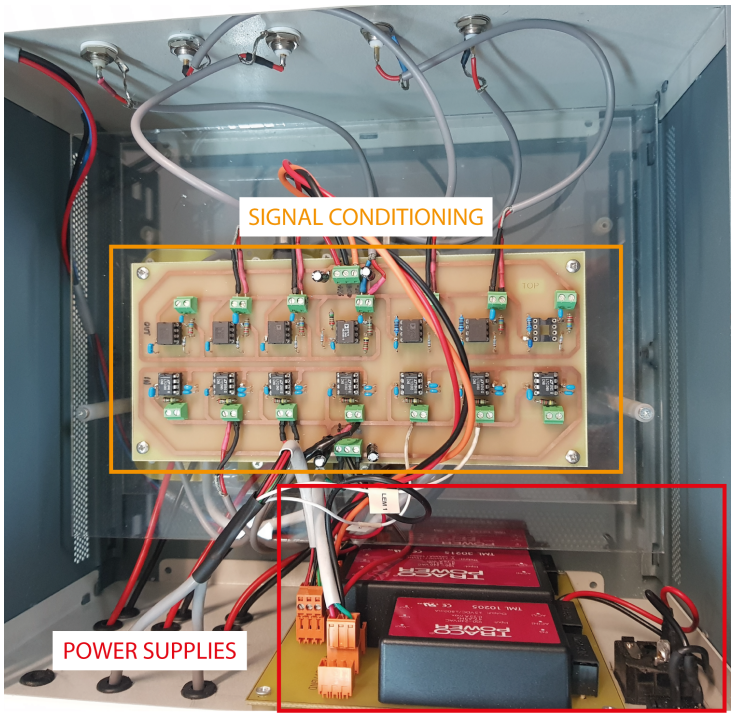

Figure 5.2: Signal conditioning module

5.1.4 Real-time simulation model in Simulink

The control was implemented in Simulink, using the structures presented in Section 4.1. However, the power structure was replaced by input and output blocks from the RTI library from dSPACE.The block diagram of the model is presented in Figure 5.3, Figure 5.4 presents the acquired signals manipulation and Figure 5.5 shows the output of the model.

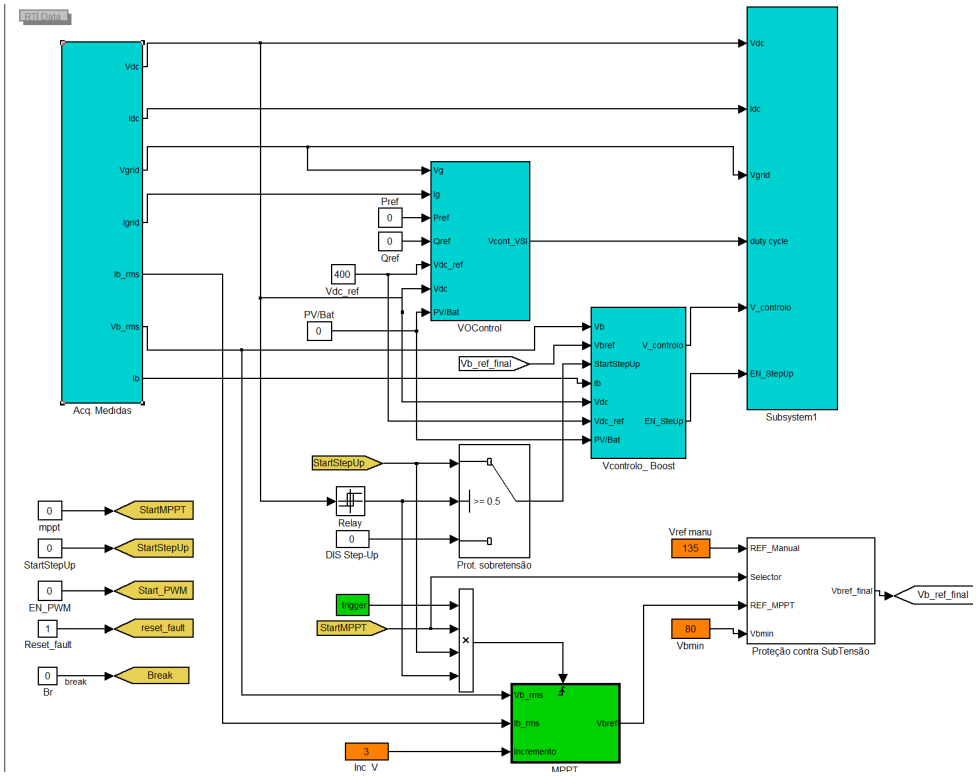

Figure 5.3: Block diagram of the model

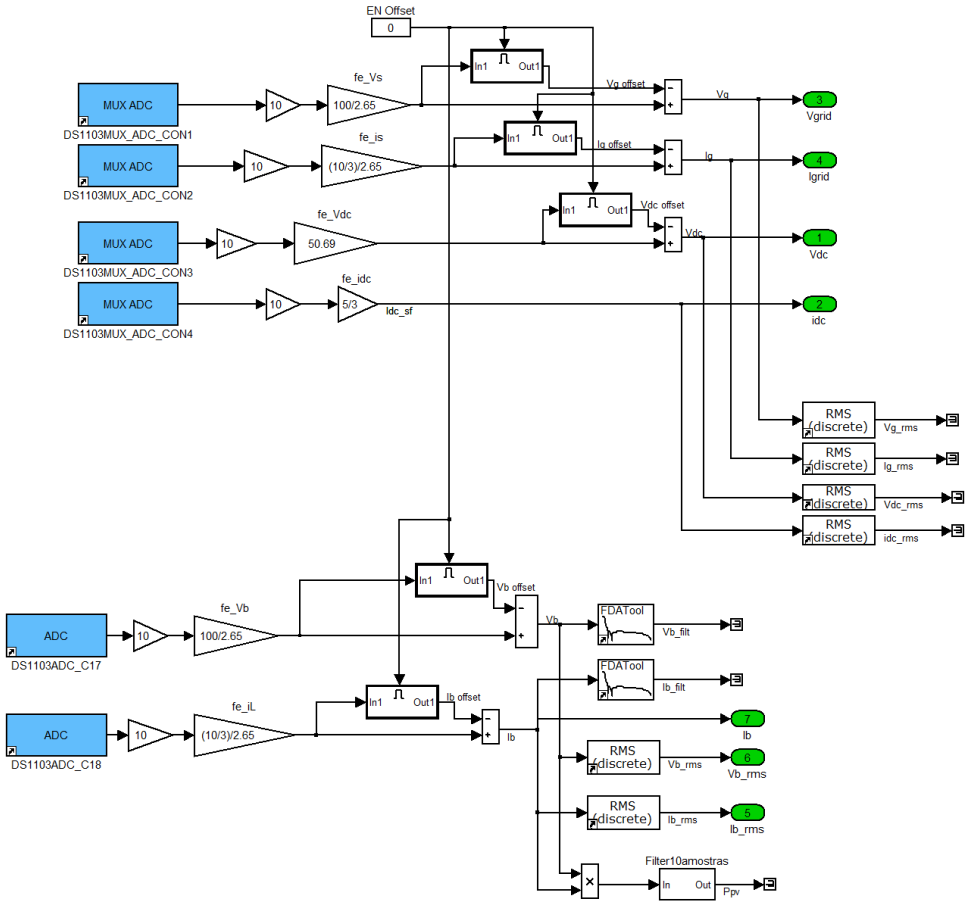

Figure 5.4: Signal manipulation

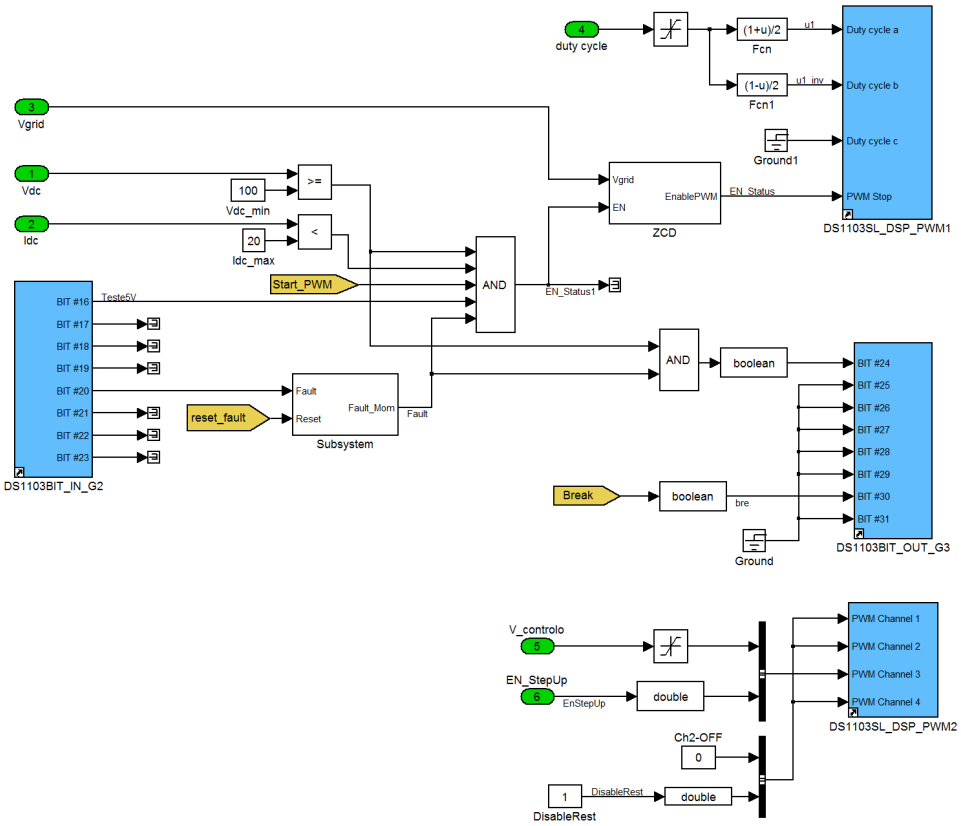

Figure 5.5: Output block

5.1.5 Assembly of a second power module and signal conditioning module

Since the presented structure has several applications, it is robust and simple to operate, it can be used in different projects at LSE. Thus, in cooperation with another student in the laboratory, was implemented a second identical platform. With this, it is possible to have simultaneously two projects using the same topology. Besides having a spare set in case of accidents that can occur in experimental tests.

5.2 Results

With the experimental platform presented in this chapter, the same tests mentioned in Chapter 4 were performed. The passive components values and controller gains were the

same as used in the simulation. One different test made was the analysis of the output current of commercial inverters that were available at LSE.

5.2.1 Comparison between PR and synchronous frame

As well as in the simulation, four different values of power were tested and the experimental results are presented in this section. The Figures 5.6 to 5.11 show the current output and the hamornic spectrum of the current together with IEEE 1547 limit values. The waveforms were obtained through dSPACE Control Desk software and the figures were plotted on Matlab.

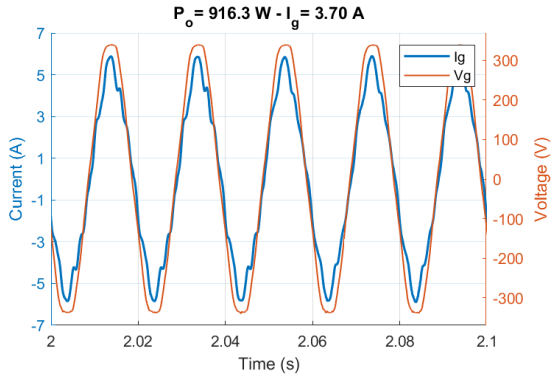

(a) PR Controller

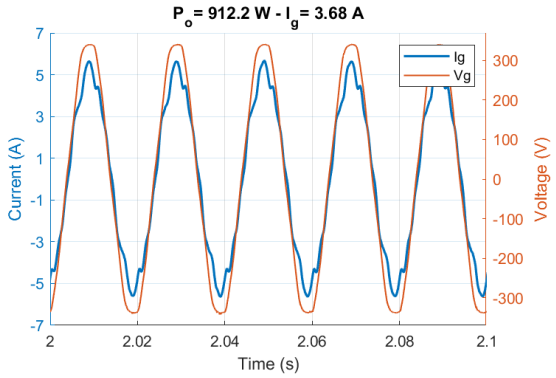

(b) PR + 3 HC

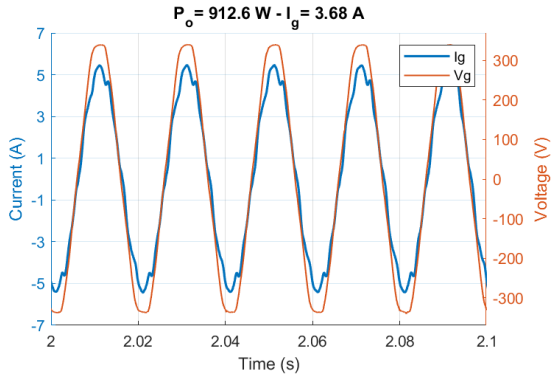

(c) PR + 3HC + 5HC

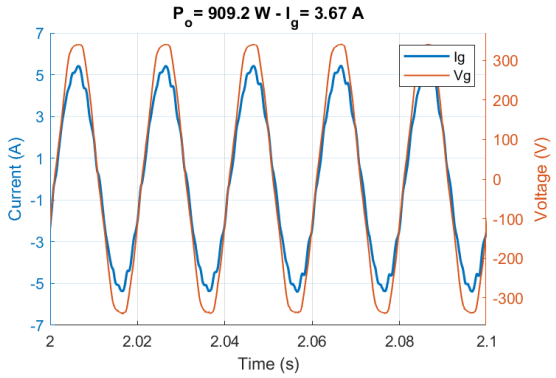

(d) PR + 3 HC + 5HC + 7HC

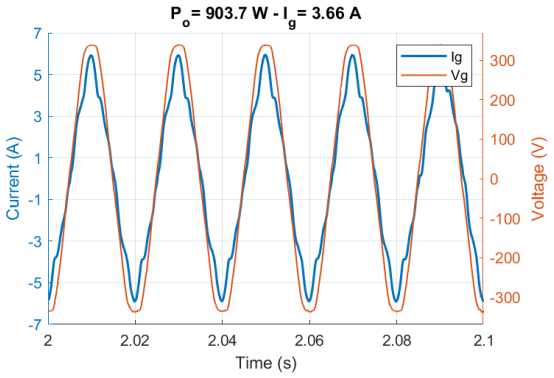

(e) Synchronous controller

Figure 5.6: Test with reference power of 1000 W

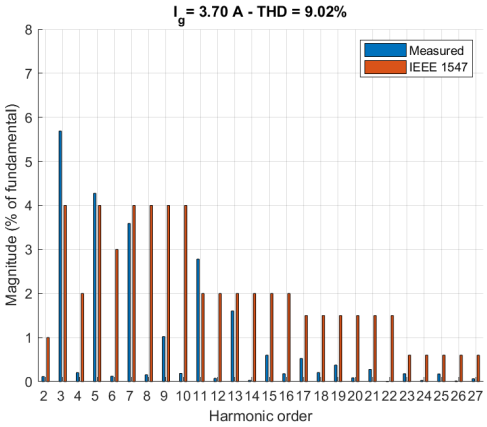

(a) PR Controller

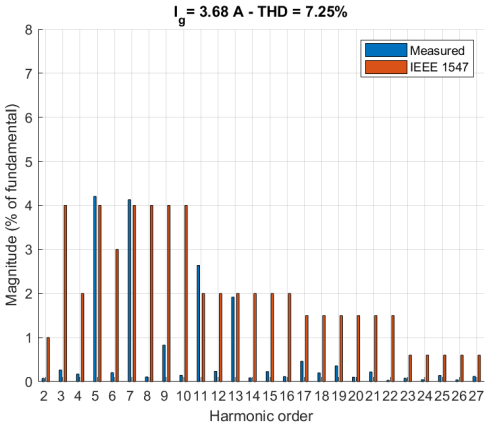

(b) PR + 3 HC

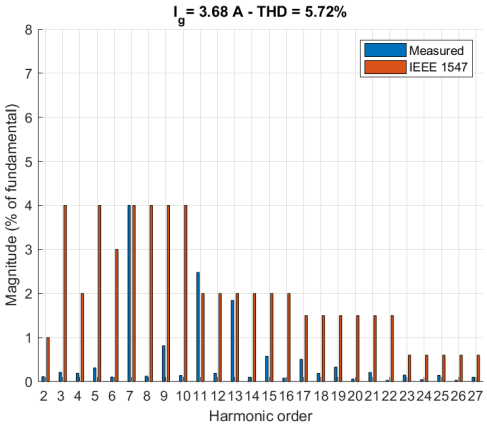

(c) PR + 3HC + 5HC

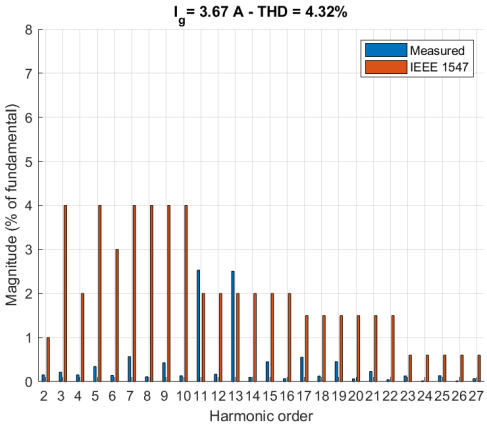

(d) PR + 3 HC + 5HC + 7HC

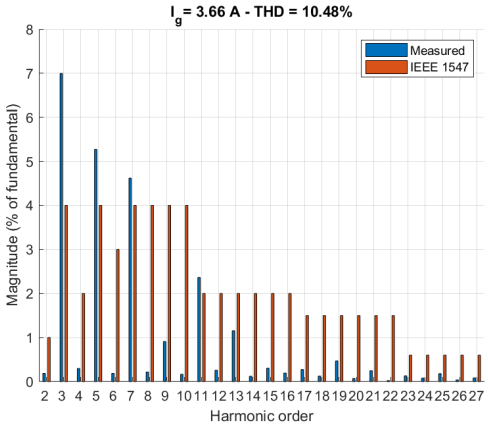

(e) Synchronous controller

Figure 5.7: Harmonics for reference power of 1000 W

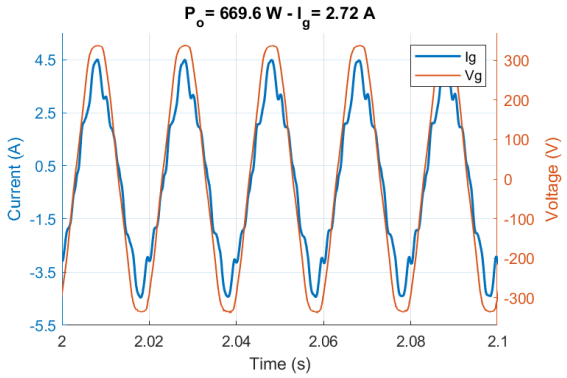

(a) PR Controller

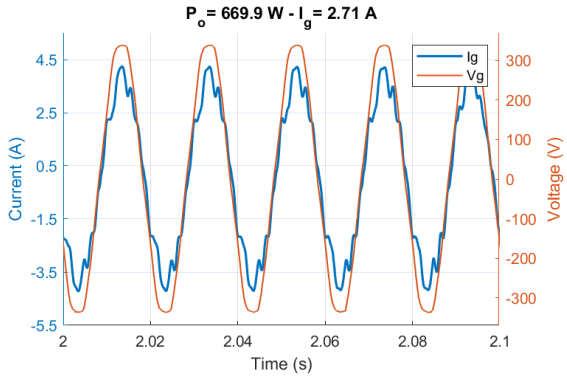

(b) PR + 3 HC

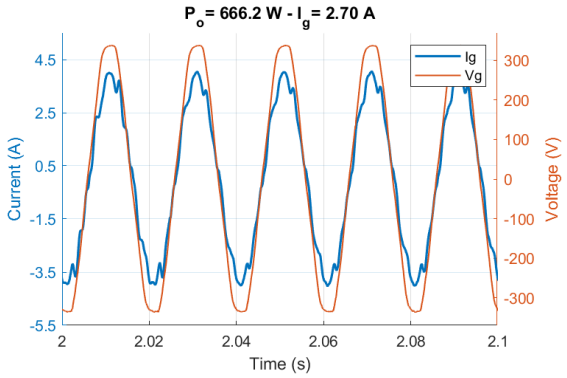

(c) PR + 3HC + 5HC

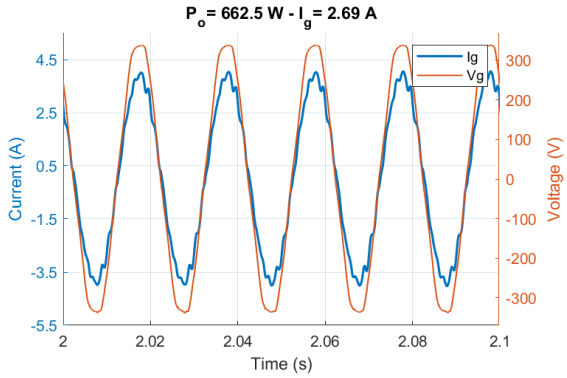

(d) PR + 3 HC + 5HC + 7HC

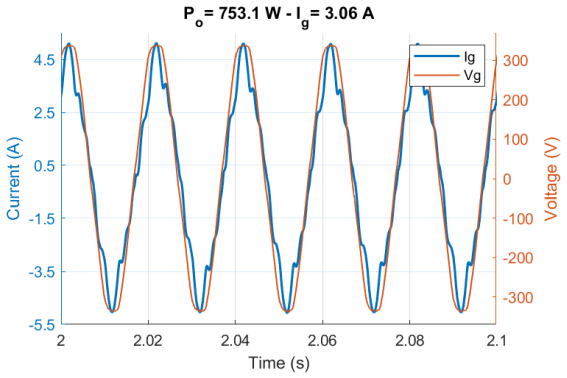

(e) Synchronous controller

Figure 5.8: Test with reference power of 750 W

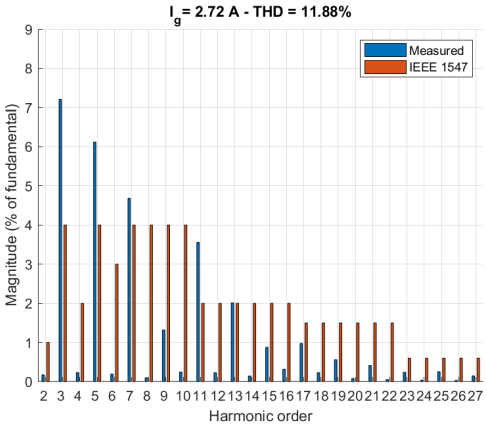

(a) PR Controller

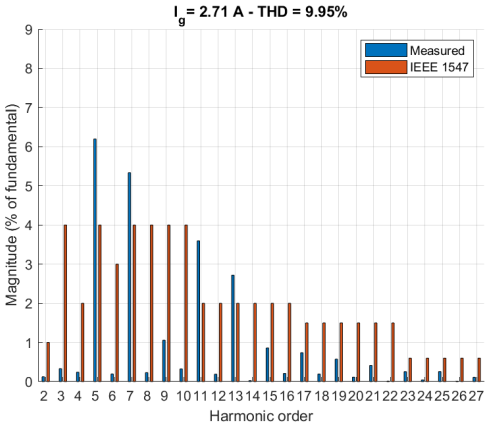

(b) PR + 3 HC

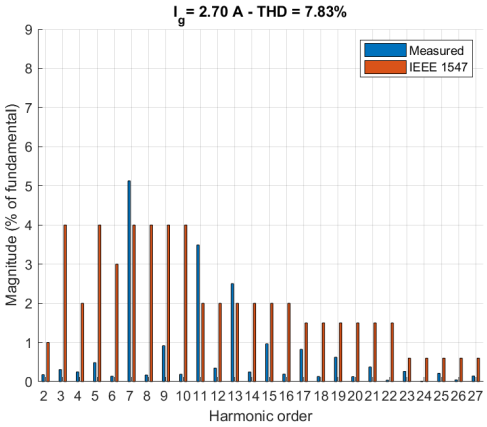

(c) PR + 3HC + 5HC

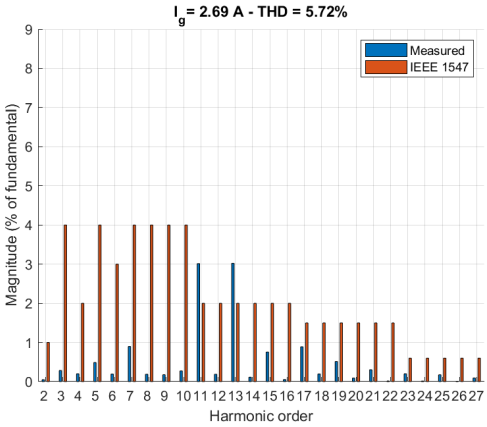

(d) PR + 3 HC + 5HC + 7HC

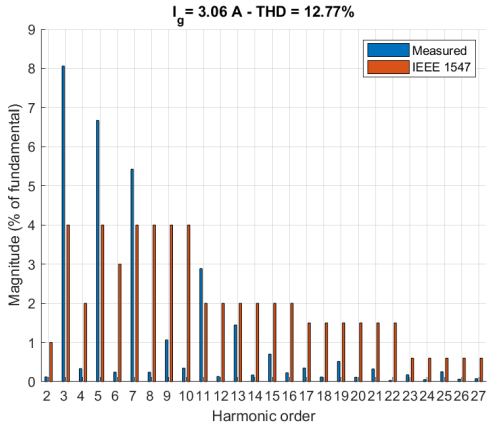

(e) Synchronous controller

Figure 5.9: Harmonics for reference power of 750 W

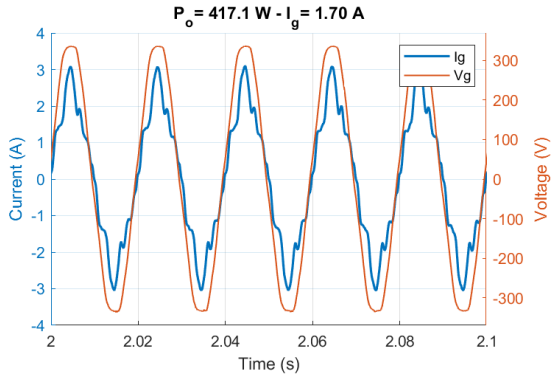

(a) PR Controller

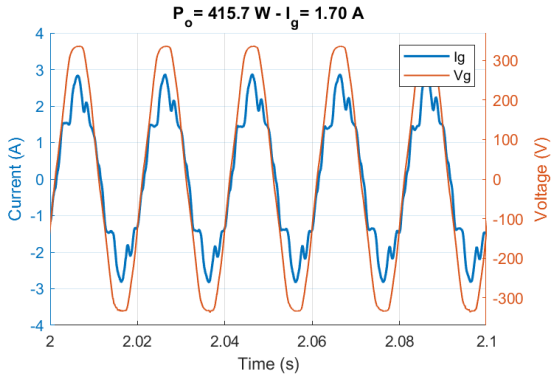

(b) PR + 3 HC

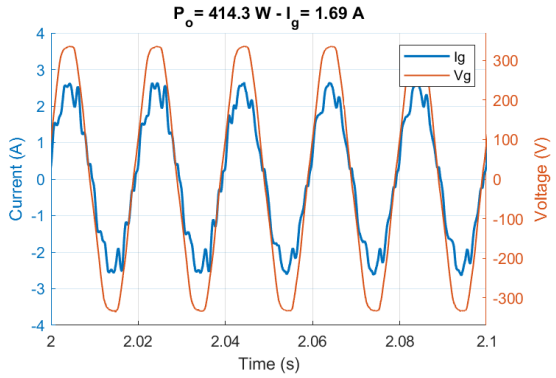

(c) PR + 3HC + 5HC

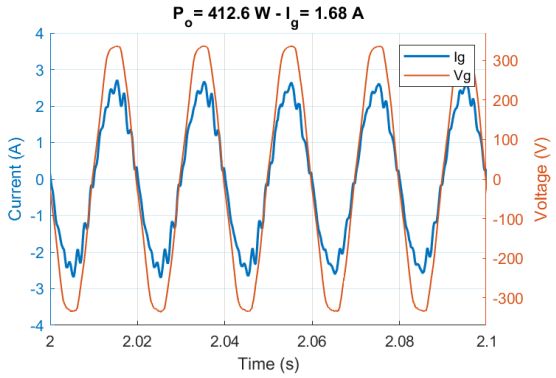

(d) PR + 3 HC + 5HC + 7HC

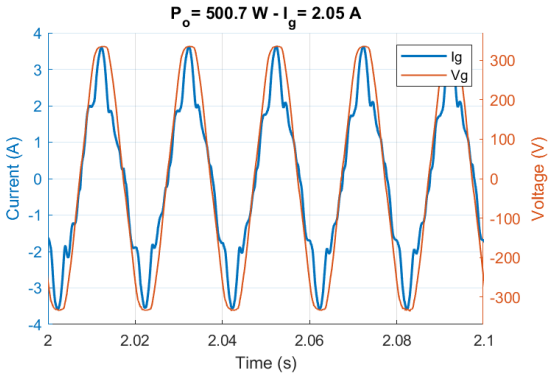

(e) Synchronous controller

Figure 5.10: Test with reference power of 500 W

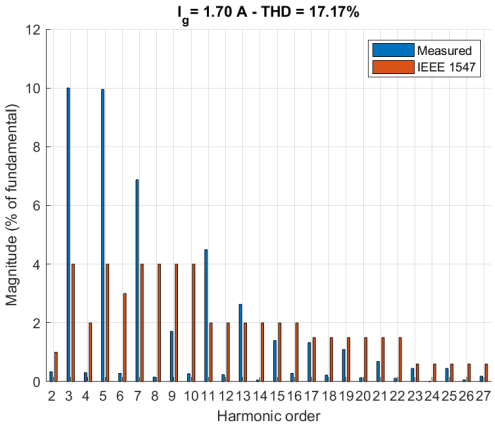

(a) PR Controller

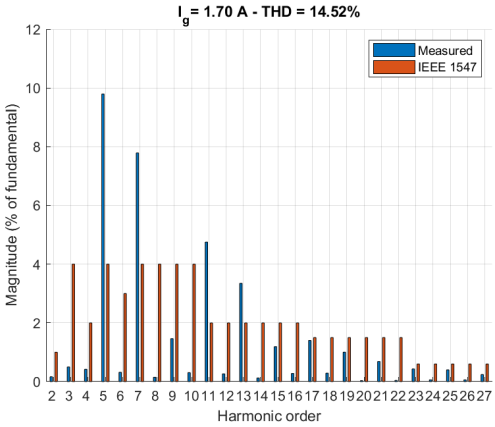

(b) PR + 3 HC

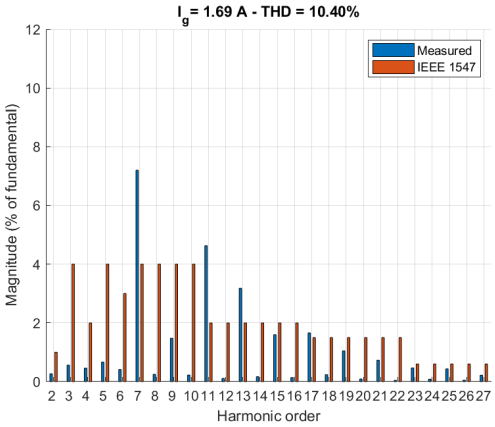

(c) PR + 3HC + 5HC

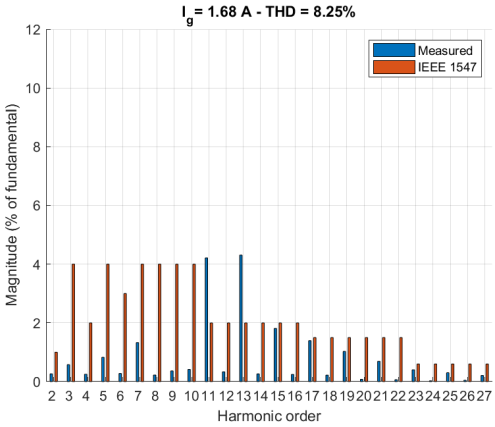

(d) PR + 3 HC + 5HC + 7HC

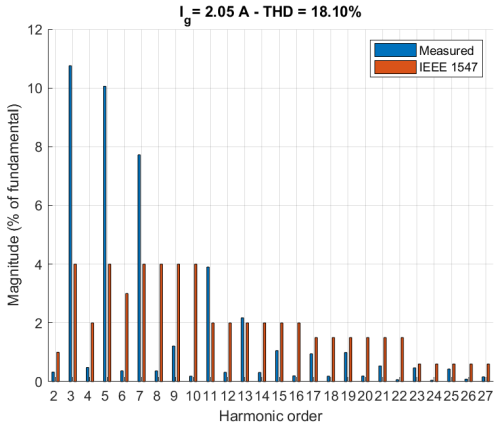

(e) Synchronous controller

Figure 5.11: Harmonics for reference power of 500 W

5.2.2 Commercial inverter analysis

Three inverters, which rated power is close to the experimental platform power, were a available in the LSE: Sunny Boy SB 1.5-1VL-40 from SMA, PIKO MP Plus 1.5-1 from Kostal, and Solis mini 700 from Ginlong. They have a rated power of 1500 W, excluding Solis mini which has only 700 W of rated power. All three have IEC 61727 certification in their datasheets, and Solis and PIKO also show a maximum current total harmonic distortion (THD) of 3%.

The tests were made on the same day, with the same PV system, and with a short time difference between them. This precautions were taken to try to avoid significant differences among the inverters injected power. The waveforms were acquired using dSPACE platform.

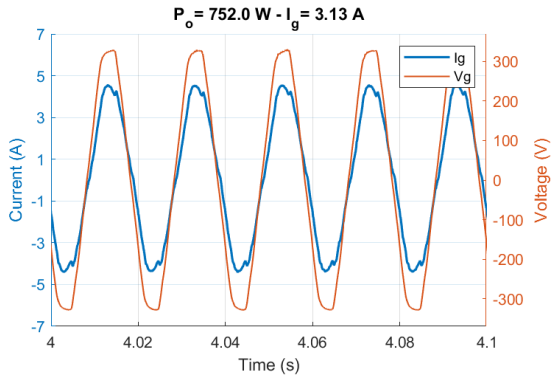

(a) Solis mini 700

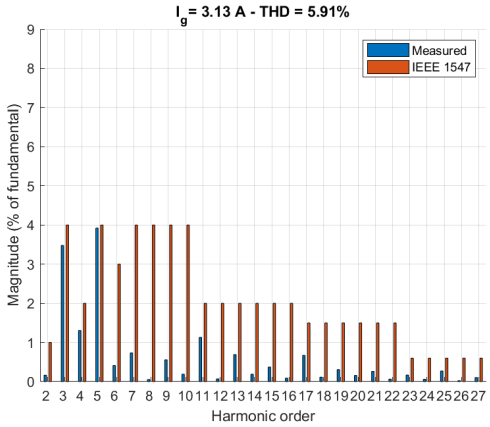

(b) Harmonics for Solis mini 700

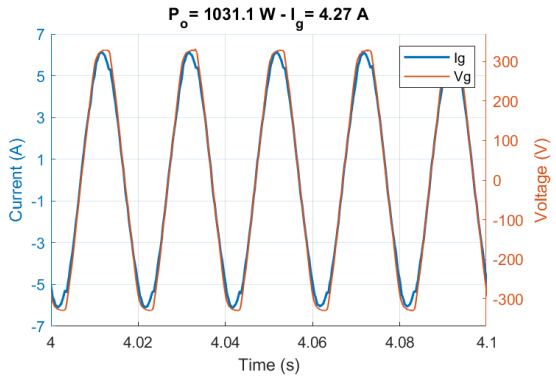

(c) PIKO MP Plus

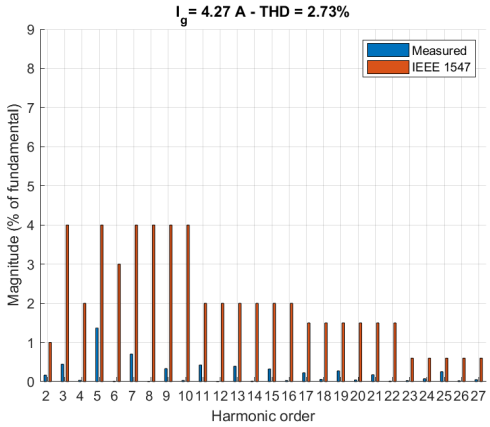

(d) Harmonics for PIKO MP Plus

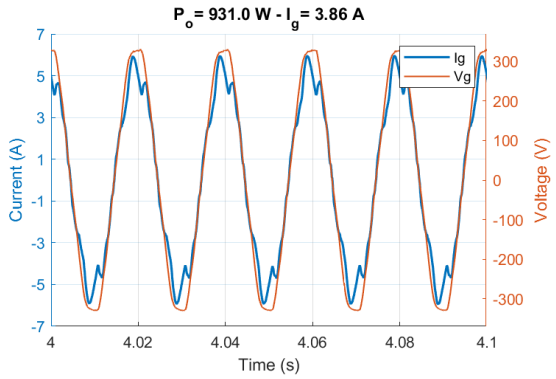

(e) Sunny Boy 1500

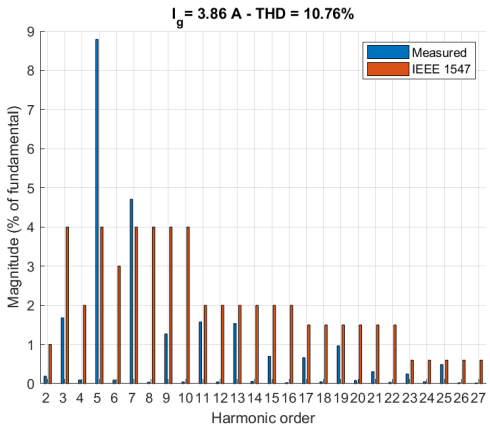

(f) Harmonics for Sunny Boy 1500

Figure 5.12: Comparison between commercial inverters

5.2.3 Tests with LC filter

To compare the performance of output filters, two different values of capacitor were applied in an LC filter: $1\mu F$ and $4.7\mu F$, similarly to the simulation test. However, the gains were the same as the test with only L filter and were not changed for the $4.7\mu F$ capacitor.

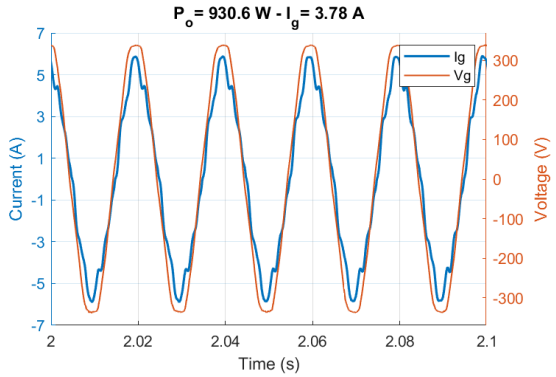

(a) PR controller and $C_f = 1\mu F$

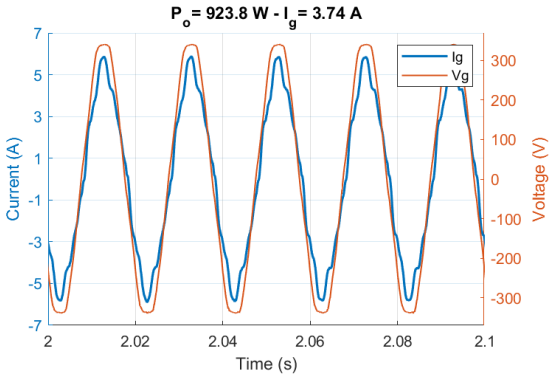

(b) PR controller and $C_f = 4.7\mu F$

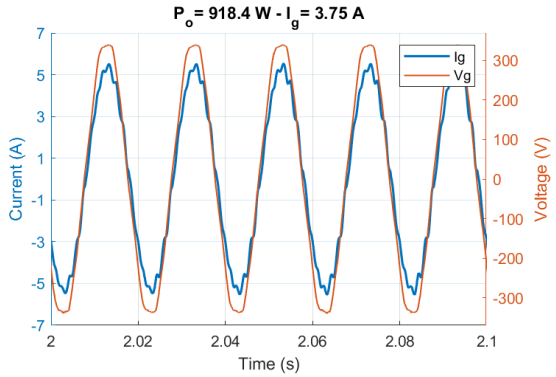

(c) PR+HC controller and $C_f = 1\mu F$

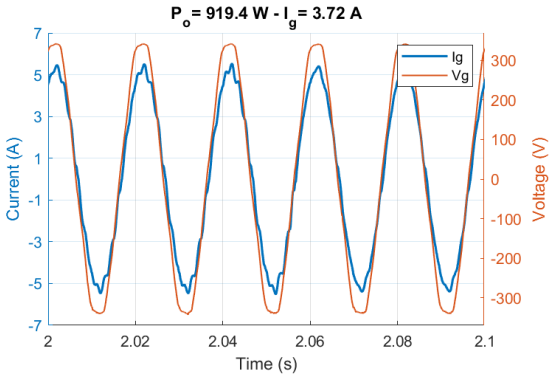

(d) PR+HC controller and $C_f = 4.7\mu F$

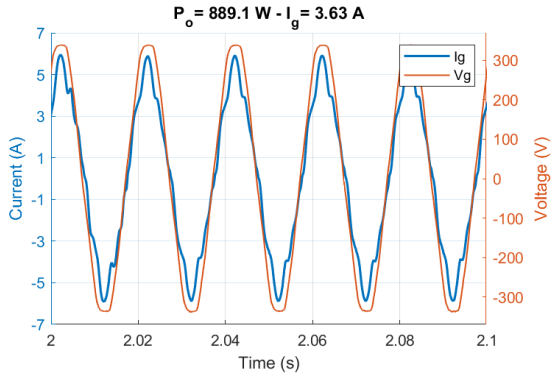

(e) Synchronous controller and $C_f = 1\mu F$

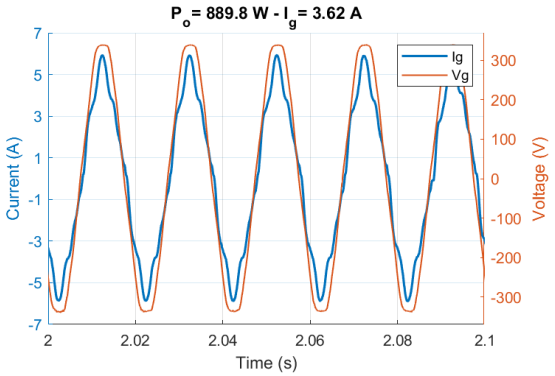

(f) Synchronous controller and $C_f = 4.7\mu F$

Figure 5.13: Test with LC filter and reference power of 1000 W

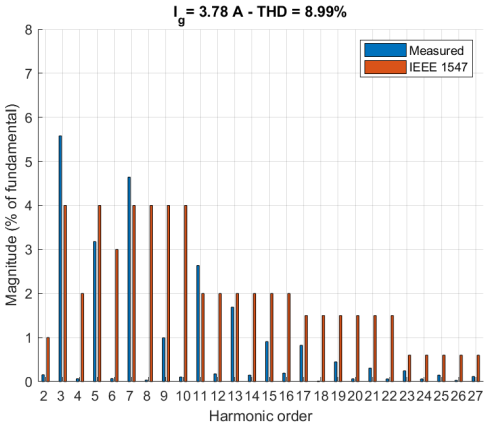

(a) PR controller and $C_f = 1\mu F$

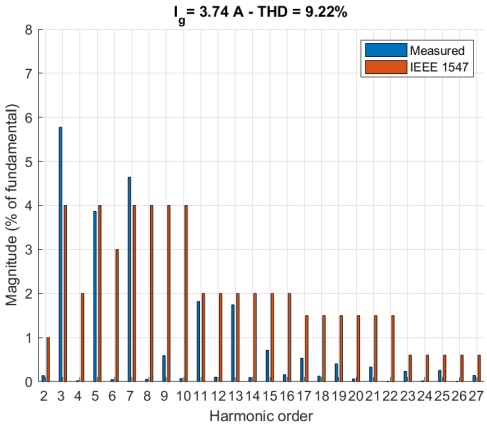

(b) PR controller and $C_f = 4.7\mu F$

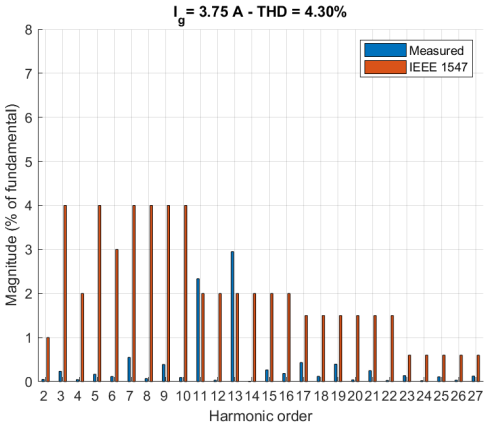

(c) PR+HC controller and $C_f = 1\mu F$

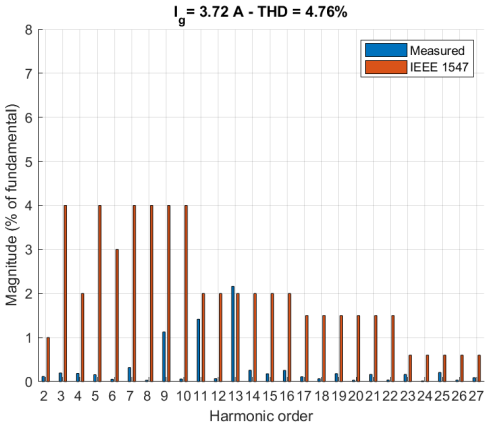

(d) PR+HC controller and $C_f = 4.7\mu F$

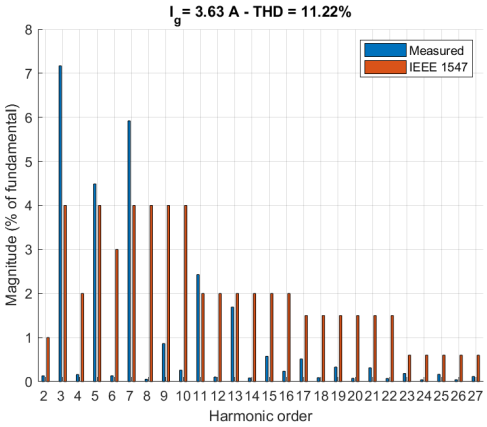

(e) Synchronous controller and $C_f = 1\mu F$

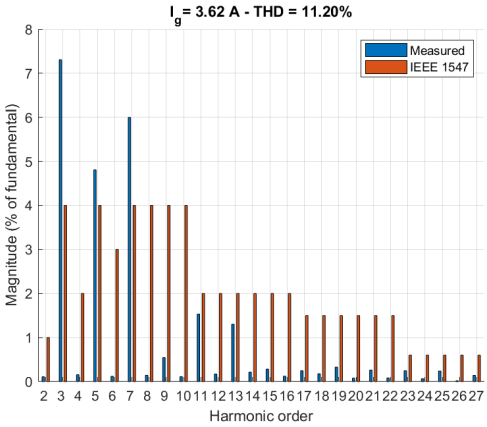

(f) Synchronous controller and $C_f = 4.7\mu F$

Figure 5.14: Harmonics for LC filter and reference power of 1000 W

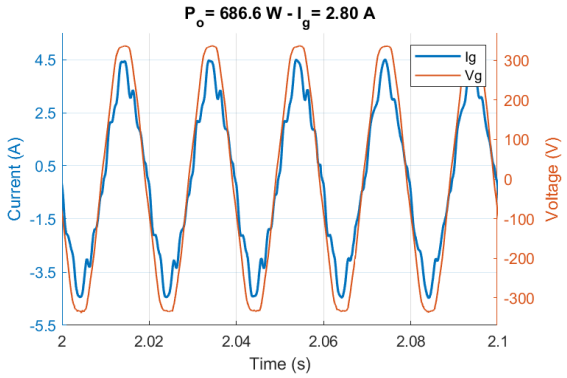

(a) PR controller and $C_f = 1\mu F$

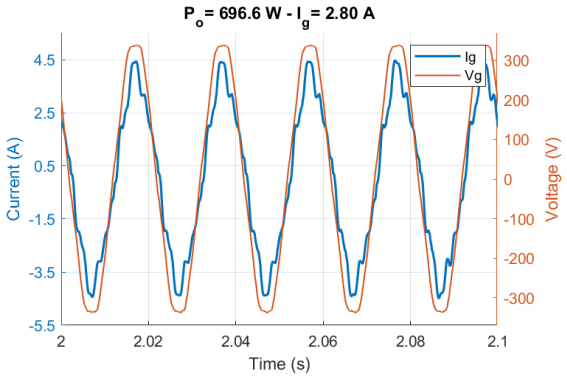

(b) PR controller and $C_f = 4.7\mu F$

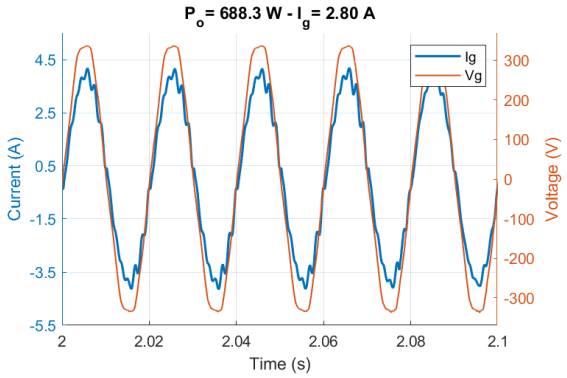

(c) PR+HC controller and $C_f = 1\mu F$

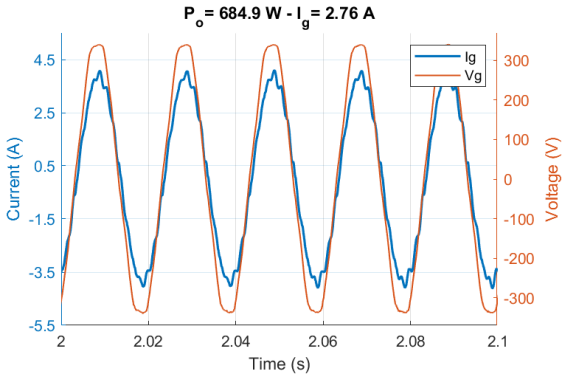

(d) PR+HC controller and $C_f = 4.7\mu F$

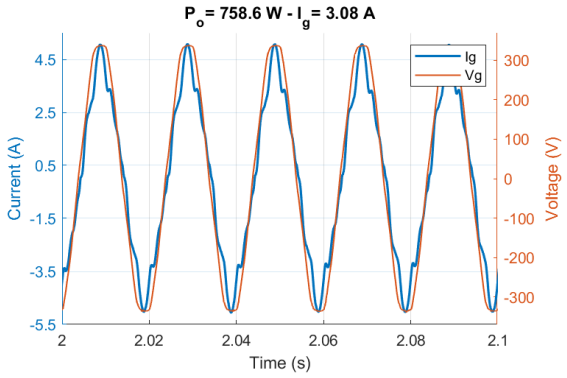

(e) Synchronous controller and $C_f = 1\mu F$

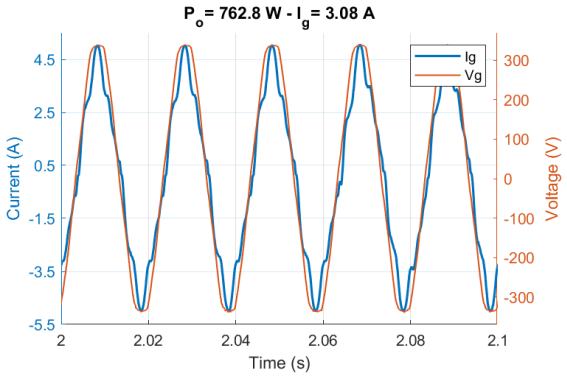

(f) Synchronous controller and $C_f = 4.7\mu F$

Figure 5.15: Test with LC filter and reference power of 750 W

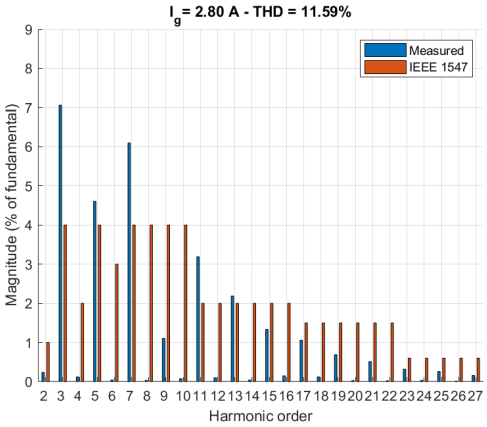

(a) PR controller and $C_f = 1\mu F$

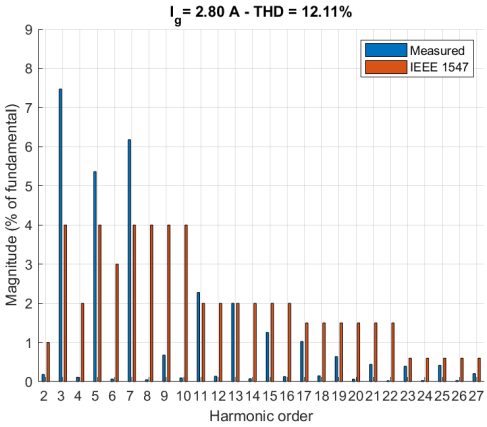

(b) PR controller and $C_f = 4.7\mu F$

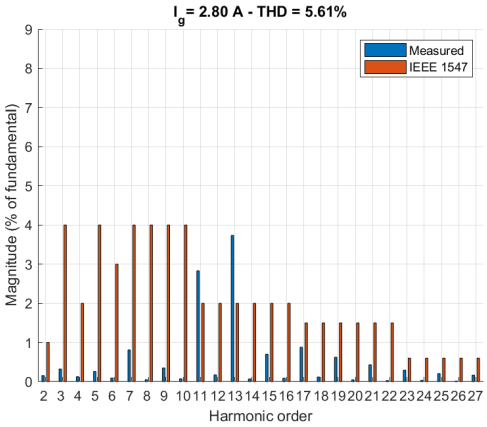

(c) PR+HC controller and $C_f = 1\mu F$

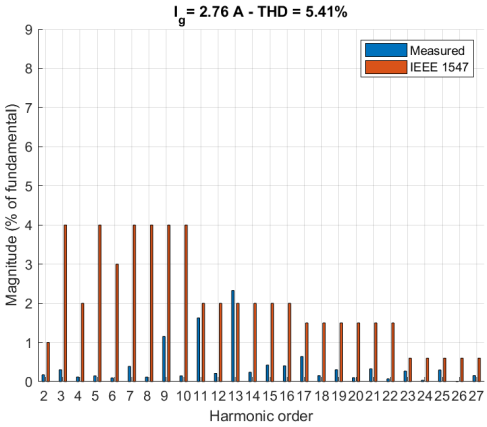

(d) PR+HC controller and $C_f = 4.7\mu F$

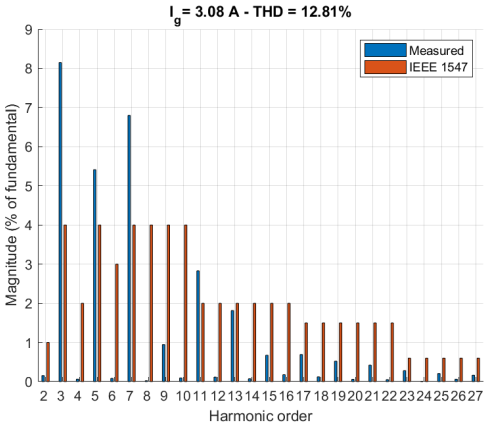

(e) Synchronous controller and $C_f = 1\mu F$

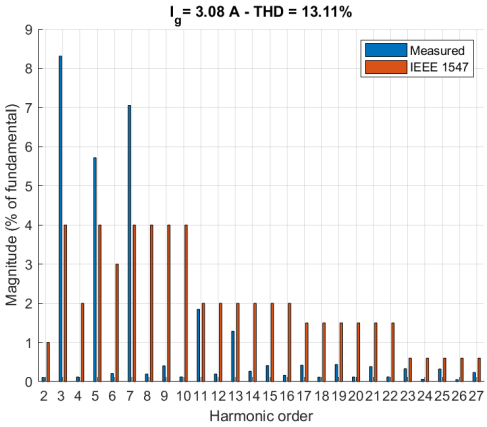

(f) Synchronous controller and $C_f = 4.7\mu F$

Figure 5.16: Harmonics for LC filter and reference power of 750 W

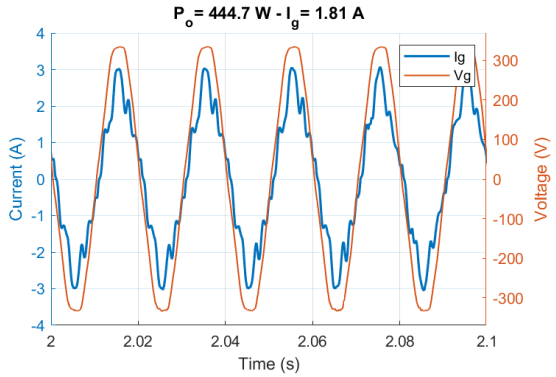

(a) PR controller and $C_f = 1\mu F$

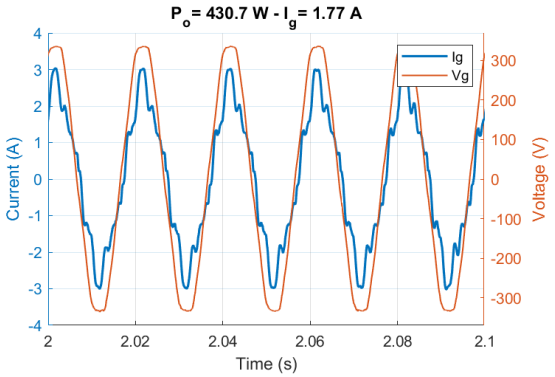

(b) PR controller and $C_f = 4.7\mu F$

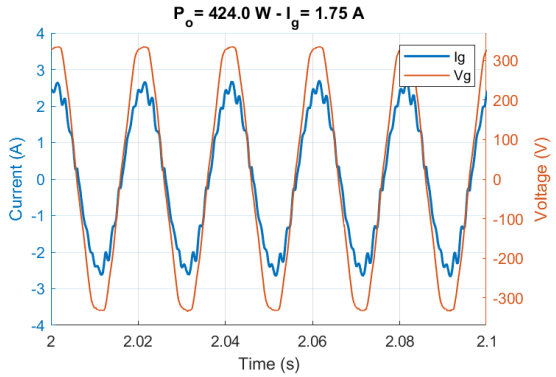

(c) PR+HC controller and $C_f = 1\mu F$

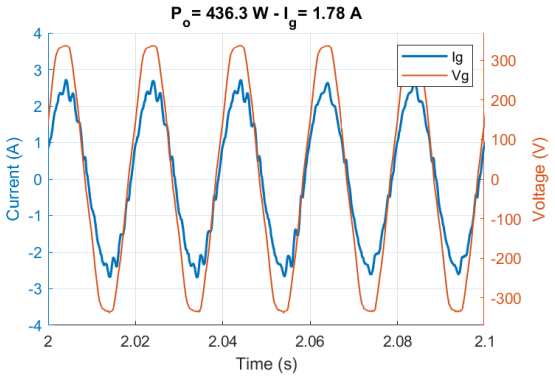

(d) PR+HC controller and $C_f = 4.7\mu F$

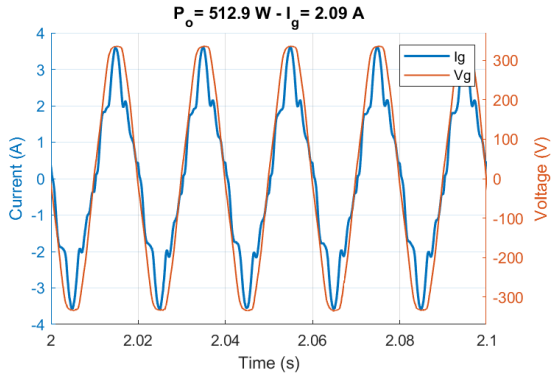

(e) Synchronous controller and $C_f = 1\mu F$

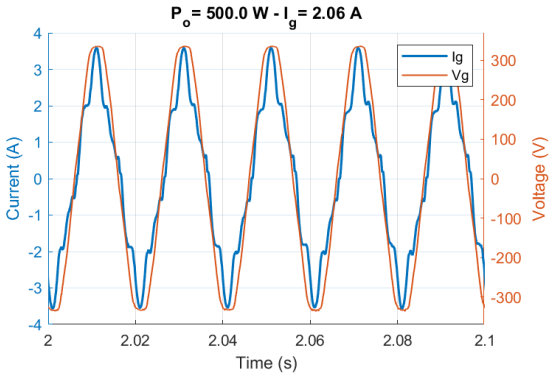

(f) Synchronous controller and $C_f = 4.7\mu F$

Figure 5.17: Test with LC filter and reference power of 500 W

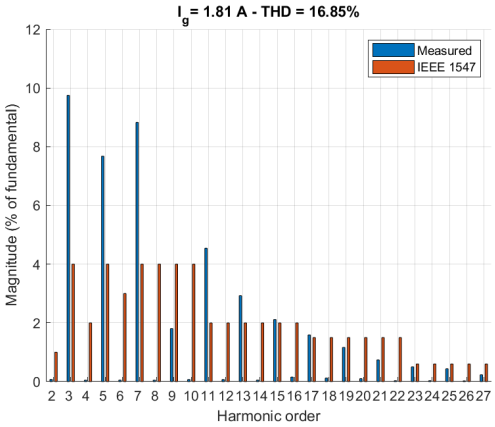

(a) PR controller and $C_f = 1\mu F$

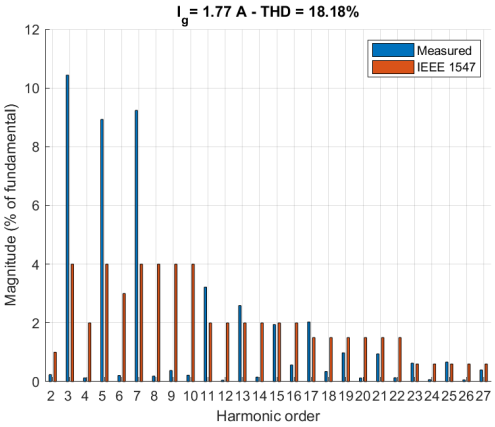

(b) PR controller and $C_f = 4.7\mu F$

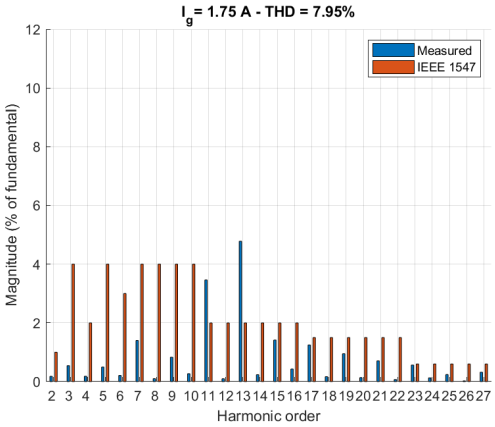

(c) PR+HC controller and $C_f = 1\mu F$

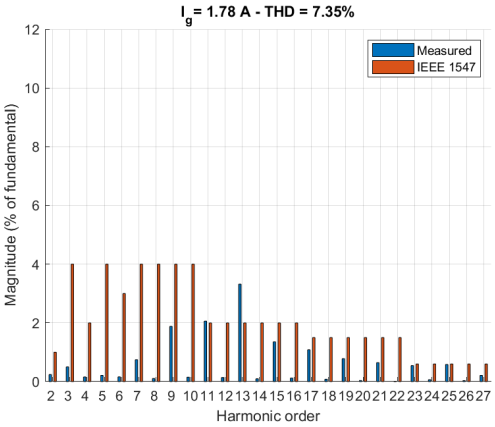

(d) PR+HC controller and $C_f = 4.7\mu F$

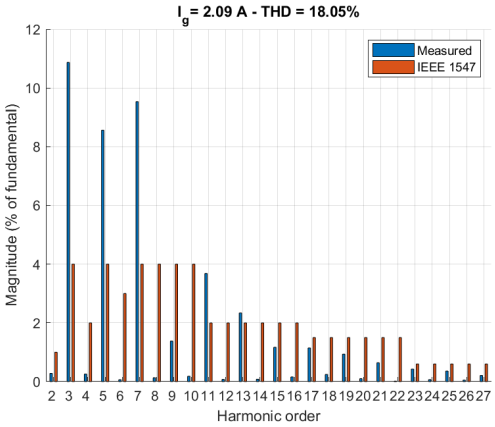

(e) Synchronous controller and $C_f = 1\mu F$

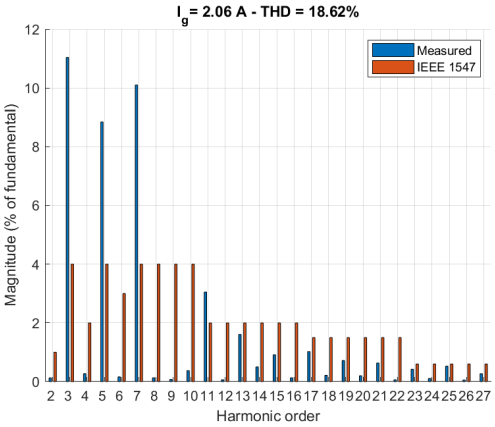

(f) Synchronous controller and $C_f = 4.7\mu F$

Figure 5.18: Harmonics for LC filter and reference power of 500 W

5.2.4 Power reference step

To properly evaluate the system stability and robustness, the output current was acquired at the moment when the inverter starts injecting power into the grid. The reference power was set at 1000 W and the waveform was recorded when the inverter IGBTs starts switching.

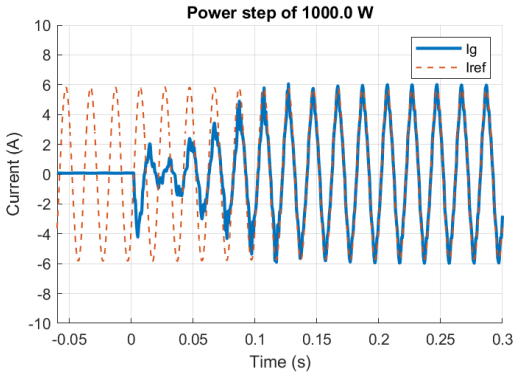

(a) PR Controller

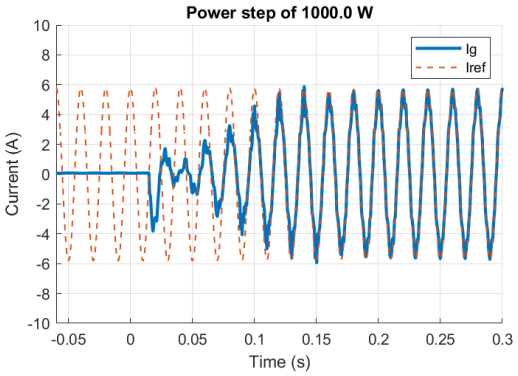

(b) PR + 3 HC

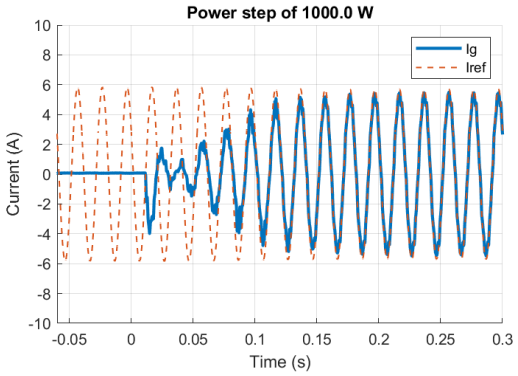

(c) PR + 3HC + 5HC

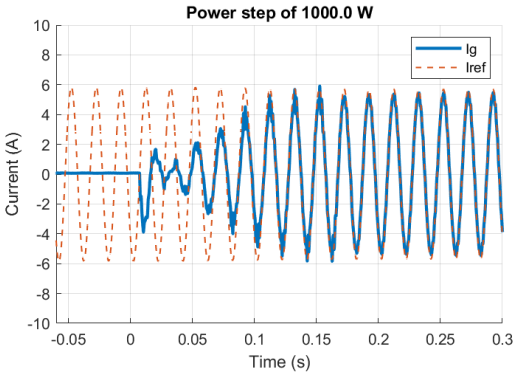

(d) PR + 3 HC + 5HC + 7HC

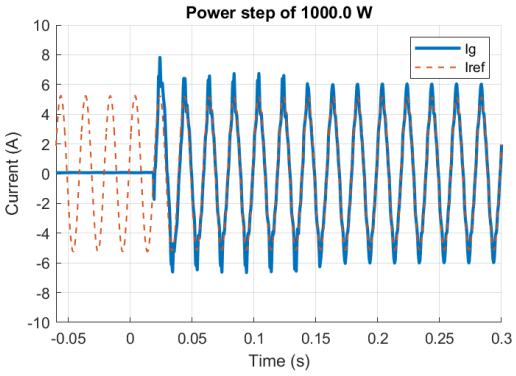

(e) Synchronous controller

Figure 5.19: Test of inverter connection to the grid

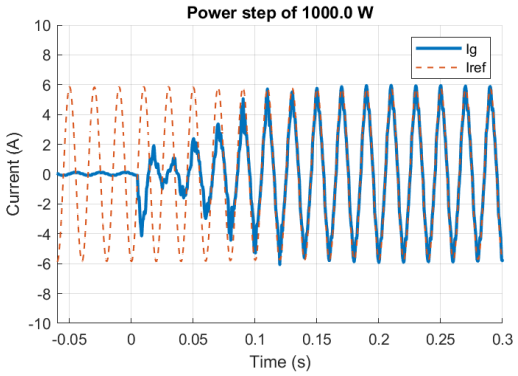

(a) PR controller and $C_f = 1\mu F$

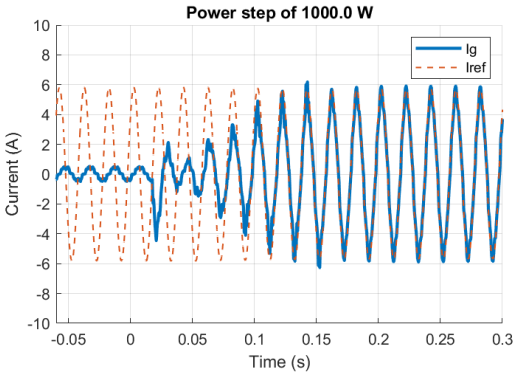

(b) PR controller and $C_f = 4.7\mu F$

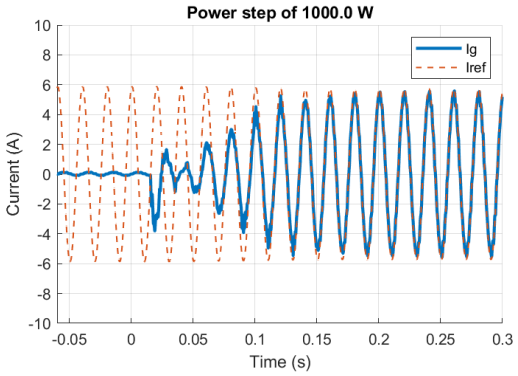

(c) PR+HC controller and $C_f = 1\mu F$

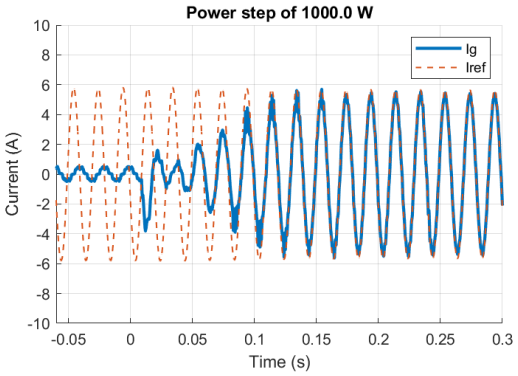

(d) PR+HC controller and $C_f = 4.7\mu F$

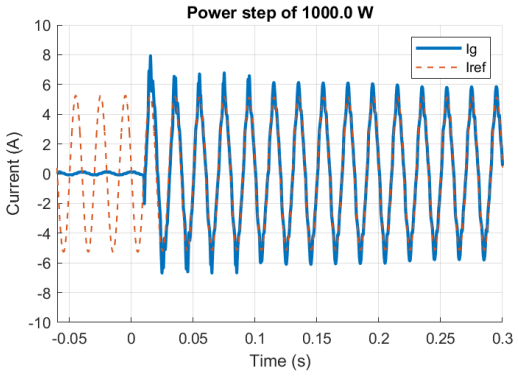

(e) Synchronous controller and $C_f = 1\mu F$

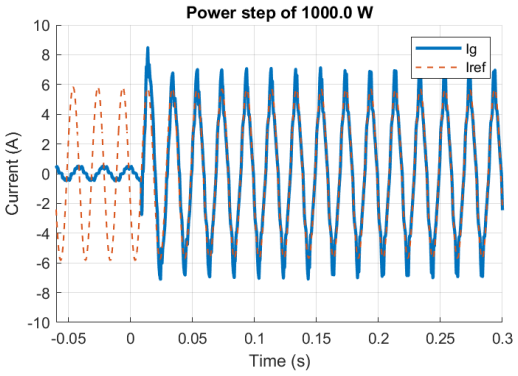

(f) Synchronous controller and $C_f = 4.7\mu F$

Figure 5.20: Test of inverter connection to the grid - With LC Filter

Chapter 6

Discussion and Analysis

With the results presented on Chapters 4 and 5 it is possible to perform an analysis over the performance of the controllers.

Observing Figures 4.8 to 4.11, which presents the current waveforms obtained in the simulation, it is clear that the current quality is lower when the injected current has a lower value. This is because the controller parameters were adjusted with an output power of 1000 W and different values will have the worst performances. The same happens in the experimental tests (Figures 5.6 to 5.11).

With the simulation, since both algorithms presented similar performance, it is not possible to determine if one is better then other. It was only possible to verify that the chosen algorithm work. However, on the practical test, the current quality changed significantly between the controllers, presenting a better THD with the PR controller than the synchronous controller, and the harmonic compensators reduced the THD even more.

Observing the harmonic spectrums presented in subsection 5.2.1, it is clear that the controllers did not respect the limits specified on IEEE 1547. This can be justified by the values of the passive components and controller gains, which was limited by the components that were available in the laboratory. Thus, the PR controller with HC only surpassed the limits for the eleventh and thirteenth harmonics at the rated power (1000 W).

Nevertheless, every harmonic compensator included takes a computational cost and spend microprocessor computing time. In the case of this work, this was not a critical point, but in housing systems or commercial applications it is important to minimize the processing time to save costs. Then, the HC may be included for the odd harmonics only to fulfill standard requirements and in the minimum quantity as possible.

Comparing with results from other works. A similar study was done in [33], a PR controller was compared to the PI controller without frame transformations and in the

output an LCL filter was used. A three-phase application, also with an LCL filter on the output, presented in [34], had lower THD values. However, the comparison results were close to the presented in this work in both of the mentioned cases.

When confronted with the commercial inverters (Figure 5.12), the results achieved in laboratory with the adopted control structure and power topology, presented comparable performance. Even though all tested inverters had harmonics compliance certificates, at the tested conditions adopted, only Kostal PIKO were in the allowed THD range.

Among the different controllers tested, the PR controller with harmonic compensation showed better current quality. However, this takes the computation time of the microcontroller and its use should be considered according to the application. Regarding only the PR compared to the synchronous controller, both have similar performance.

Concerning the LC filter, it presented a slight improvement on current quality on practical tests. By the analysis of the harmonic spectrum, it is noticed that higher filter capacitance can attenuate higher orders harmonics (i.e. 11^{th} and 13^{th}). But as well as the harmonic compensators, a cost analysis should be done. The number of passive components, especially the inductor, directly affects product costs, efficiency and weight.

The results presented in subsection 5.2.4 shows that the system is stable even in transients. For the PR controller and the PR+HC controller, almost no overshoot was noted and the current stabilized in around 9 cycles (0.18 s). The synchronous controller had an overshoot of approximately 30%, but the settling time was of 7 cycles (0.14 s).

Chapter 7

Conclusions

The inverters that integrate DG systems can inject harmonics and reduce power quality. Acknowledging the expansion of the number of renewable energy sources connected to the grid, it is important to investigate methods to improve the quality of the injected power.

The studied techniques were implemented in both computational and experimental platforms. Two control structures and two different filter topologies were tested. Additionally, a second experimental platform was assembled, that will allow LSE to have more projects simultaneously.

The test and analysis of different control structures for grid-connected inverters and output filter topologies were successful. Both experimental and simulation implementations proposed were tested and validated on different power values, proving system stability on variable conditions.

The PR controller and the synchronous controller were tested, as well as the harmonic compensators. All implemented control algorithms proved to be functional and appropriate for voltage source inverter control. In an overall analysis, the PR controller with harmonic compensation presented better results. But only the PR controller or the synchronous controller had satisfactory results.

The selection of the control algorithm for the inverter should be done considering the expected performance of the converter and available computational power. For simpler applications, the PI controller in the synchronous frame can be used. But for a more complex system, the PR controller with HC should be a better choice.

Regarding the analysis of the output filter, it was noted that the control is affected by the filter. Topology and values change system behavior and may lead to instability. Nevertheless, both L and LC filters were tested and presented acceptable results. Cost and efficiency should be analyzed to select the best filter configuration according to the application.

7.1 Future work

This section proposes future works that can be done related to this research theme. To determine and investigate better solutions to grid-connected inverter control and current quality.

- Test controllers and output filter with reactive power exchange with the grid;
- Implement control structures in a digital signal processor (DSP) instead of dSPACE Controller board to investigate and compare the computational time of the controllers;
- Use LCL filter and analyze its performance;
- Investigate and implement more recent and not fully developed control structures of inverter's current.

References

[1] H. Ritchie and M. Roser, "Energy", *Our World in Data*, 2020, https://ourworldindata.org/energy.

[2] W. Xiong, J. Zeng, L. Wu, and H. Cheng, "Power management of a residential hybrid photovoltaic inverter with battery energy storage system", in *2019 IEEE 10th International Symposium on Power Electronics for Distributed Generation Systems (PEDG)*, IEEE, 2019, pp. 450–454.

[3] A. G. Tsikalakis and N. D. Hatziargyriou, "Centralized control for optimizing microgrids operation", in *2011 IEEE power and energy society general meeting*, IEEE, 2011, pp. 1–8.

[4] J. Gallardo-Lozano, E. Romero-Cadaval, V. Miñambres-Marcos, D. Vinnikov, T. Jalakas, and H. Hõimoja, "Grid reactive power compensation by using electric vehicles", in *2014 Electric Power Quality and Supply Reliability Conference (PQ)*, IEEE, 2014, pp. 19–24.

[5] P. Rodriguez, A. V. Timbus, R. Teodorescu, M. Liserre, and F. Blaabjerg, "Flexible active power control of distributed power generation systems during grid faults", *IEEE transactions on industrial electronics*, vol. 54, no. 5, pp. 2583–2592, 2007.

[6] S. K. Khadem, M. Basu, and M. Conlon, "Power quality in grid connected renewable energy systems: Role of custom power devices", 2010.

[7] R. I. Bojoi, L. R. Limongi, D. Roiu, and A. Tenconi, "Enhanced power quality control strategy for single-phase inverters in distributed generation systems", *IEEE Transactions on Power Electronics*, vol. 26, no. 3, pp. 798–806, 2011.

[8] T. E. McDermott and R. C. Dugan, "Distributed generation impact on reliability and power quality indices", in *2002 Rural Electric Power Conference. Papers Presented at the 46th Annual Conference (Cat. No. 02CH37360)*, IEEE, 2002, pp. D3–1.

[9] I. Hernando-Gil, I.-S. Ilie, A. J. Collin, J. L. Acosta, and S. Z. Djokic, "Impact of dg and energy storage on distribution network reliability: A comparative analysis", in *2012 IEEE international energy conference and exhibition (ENERGYCON)*, IEEE, 2012, pp. 605–611.

[10] F. Blaabjerg, R. Teodorescu, M. Liserre, and A. V. Timbus, "Overview of control and grid synchronization for distributed power generation systems", *IEEE Transactions on industrial electronics*, vol. 53, no. 5, pp. 1398–1409, 2006.

[11] R. Teodorescu, M. Liserre, and P. Rodriguez, *Grid converters for photovoltaic and wind power systems*. John Wiley & Sons, 2011, vol. 29.

[12] R. C. Dugan, T. S. Key, and G. J. Ball, "Distributed resources standards", *IEEE Industry Applications Magazine*, vol. 12, no. 1, pp. 27–34, 2006.

[13] T. S. Basso and R. DeBlasio, "Ieee 1547 series of standards: Interconnection issues", *IEEE Transactions on Power Electronics*, vol. 19, no. 5, pp. 1159–1162, 2004.

[14] K. Ogata and Y. Yang, *Modern control engineering*, 5th ed. Prentice hall Upper Saddle River, NJ, 2010.

[15] B. Bahrani, A. Rufer, S. Kenzelmann, and L. A. Lopes, "Vector control of single-phase voltage-source converters based on fictive-axis emulation", *IEEE Transactions on Industry Applications*, vol. 47, no. 2, pp. 831–840, 2010.

[16] S Samerchur, S Premrudeepreechacharn, Y Kumsuwun, and K Higuchi, "Power control of single-phase voltage source inverter for grid-connected photovoltaic systems", in *2011 IEEE/PES Power Systems Conference and Exposition*, IEEE, 2011, pp. 1–6.

[17] R. Zhang, M. Cardinal, P. Szczesny, and M. Dame, "A grid simulator with control of single-phase power converters in dq rotating frame", in *2002 IEEE 33rd Annual IEEE Power Electronics Specialists Conference. Proceedings (Cat. No. 02CH37289)*, IEEE, vol. 3, 2002, pp. 1431–1436.

[18] R. Teodorescu, F. Blaabjerg, M. Liserre, and P. C. Loh, "Proportional-resonant controllers and filters for grid-connected voltage-source converters", *IEE Proceedings-Electric Power Applications*, vol. 153, no. 5, pp. 750–762, 2006.

[19] M.-H. Jahanbakhshi, B. Asaei, and B. Farhangi, "A novel deadbeat controller for single phase pv grid connected inverters", in *2015 23rd Iranian Conference on Electrical Engineering*, IEEE, 2015, pp. 1613–1617.

[20] B. Farhangi, "A novel modified deadbeat controller for vehicle to grid application", in *The 6th Power Electronics, Drive Systems & Technologies Conference (PEDSTC2015)*, IEEE, 2015, pp. 47–52.

[21] S. Hara, Y. Yamamoto, T. Omata, and M. Nakano, "Repetitive control system: A new type servo system for periodic exogenous signals", *IEEE Transactions on automatic control*, vol. 33, no. 7, pp. 659–668, 1988.

[22] H. L. Broberg and R. G. Molyet, "Reduction of repetitive errors in tracking of periodic signals: Theory and application of repetitive control", in *[Proceedings 1992] The First IEEE Conference on Control Applications*, IEEE, 1992, pp. 1116–1121.

[23] M. Büyük, A. Tan, M. Tümay, and K. Ç. Bayındır, "Topologies, generalized designs, passive and active damping methods of switching ripple filters for voltage source inverter: A comprehensive review", *Renewable and Sustainable Energy Reviews*, vol. 62, pp. 46–69, 2016.

[24] H. Cha and T.-K. Vu, "Comparative analysis of low-pass output filter for single-phase grid-connected photovoltaic inverter", in *2010 Twenty-Fifth Annual IEEE Applied Power Electronics Conference and Exposition (APEC)*, IEEE, 2010, pp. 1659–1665.

[25] Y. Tang, P. C. Loh, P. Wang, F. H. Choo, and F. Gao, "Exploring inherent damping characteristic of lcl-filters for three-phase grid-connected voltage source inverters", *IEEE Transactions on Power Electronics*, vol. 27, no. 3, pp. 1433–1443, 2011.

[26] M. M. Breve, "Implementation of a bidirectional grid interface for an electric vehicle", PhD thesis, 2019.

[27] L. C. d. Silva, "Power interface for grid-connected pico-hydro systems using pv inverters", PhD thesis, 2019.

[28] J. J. T. Coelho, "Control of a bidirectional dc-dc converter for grid-connected electric vehicles", PhD thesis, 2020.

[29] C. Wang, X. Yin, M. Wen, J. Liu, Q. Xiong, and B. Zhang, "Structure and parameters design of output lc filter in d-statcom", in *2010 International Conference on Power System Technology*, IEEE, 2010, pp. 1–6.

[30] M. Ciobotaru, R. Teodorescu, and F. Blaabjerg, "A new single-phase pll structure based on second order generalized integrator", in *2006 37th IEEE Power Electronics Specialists Conference*, IEEE, 2006, pp. 1–6.

[31] R. Teodorescu, F. Blaabjerg, U. Borup, and M. Liserre, "A new control structure for grid-connected lcl pv inverters with zero steady-state error and selective harmonic compensation", in *Nineteenth Annual IEEE Applied Power Electronics Conference and Exposition, 2004. APEC'04.*, IEEE, vol. 1, 2004, pp. 580–586.

[32] S. A. Richter and R. W. De Doncker, "Digital proportional-resonant (pr) control with anti-windup applied to a voltage-source inverter", in *Proceedings of the 2011 14th European Conference on Power Electronics and Applications*, IEEE, 2011, pp. 1–10.

[33] H. Cha, T.-K. Vu, and J.-E. Kim, "Design and control of proportional-resonant controller based photovoltaic power conditioning system", in *2009 IEEE Energy Conversion Congress and Exposition*, IEEE, 2009, pp. 2198–2205.

[34] A. Timbus, M. Liserre, R. Teodorescu, P. Rodriguez, and F. Blaabjerg, "Evaluation of current controllers for distributed power generation systems", *IEEE Transactions on power electronics*, vol. 24, no. 3, pp. 654–664, 2009.